8-2017

Modeling Ozark Caves with Structure-from-Motion Photogrammetry: An Assessment of Stand-Alone Photogrammetry for 3-Dimensional Cave Survey

Joseph H. Jordan
University of Arkansas, Fayetteville

Modeling Ozark Caves with Structure-from-Motion Photogrammetry: An Assessment of Stand-Alone Photogrammetry for 3-Dimensional Cave Survey

A thesis submitted in partial fulfillment
of the requirements for the degree of
Master of Science in Geography

by

Joseph Jordan
Arkansas Tech University
Bachelor of Science in Geology, 2015

August 2017
University of Arkansas

This thesis is approved for recommendation to the Graduate Council.

Dr. Jackson Cothren
Thesis Director

Dr. Mathew Covington
Committee Member

Dr. W. Fred Limp
Committee Member

Abstract

Nearly all aspects of karst science and management begin with a map. Yet despite this fact, cave survey is largely conducted in the same archaic way that is has been for years - with a compass, tape measure, and a sketchpad. Traditional cave survey can establish accurate survey lines quickly. However, passage walls, ledges, profiles, and cross-sections are time intensive and ultimately rely on the sketcher's experience at interpretively hand drawing these features between survey stations.

This project endeavors to experiment with photogrammetry as a method of improving on traditional cave survey, while also avoiding some of the major pitfalls of terrestrial laser scanning. The proposed method allows for the creation of 3D models which capture cave wall geometry, important cave formations, as well as providing the ability to create cross sections anywhere desired. The interactive 3D cave models are produced cheaply, with equipment that can be operated in extremely confined, harsh conditions, by unpaid volunteers with little to no technical training.

While the rapid advancement of photogrammetric software has led to its use in many 3D modeling applications, there is only a sparse body of research examining the use of photogrammetry as a standalone method for surveying caves. The proposed methodology uses a GoPro camera and a 1000 lumen portable floodlight to capture still images down the length of cave passages. The procedure goes against several traditional rules of thumb, both operating in the dark with a moving light source, as well as utilizing a wide angle, fish eye lens, to capture scene information that is not perpendicular to the camera's field of view. Images are later processed into 3D models using Agisoft's PhotoScan.

Four caves were modeled using the method, with varying levels of success. The best results occurred in dry confined passages, while passages greater than 9 meters (30ft) in width, or those with a great deal of standing water in the floor, produced large holes. An additional experiment occurred in the University of Arkansas utility tunnel.

Acknowledgments

There is a long list of people who made this project possible. First and for most, I would like to express my deep gratitude to my committee members Dr. Mathew Covington, Dr. Fred Limp, and especially to my advisor Dr. Jack Cothren, for their continued support and guidance throughout the research.

Also of paramount importance were the cave owners and park/plant managers, most of which did not know me well at the time, but none the less were excited to be a part of this experimental research. Specifically, I would like to thank Rita Smith, Faron Usrey, Caven Clark, Brian Culpepper, and Doug Moore, who were all key in helping to grant me access to each of the various study sites.

I am incredibly grateful to the University of Arkansas and the Center for Advanced Spatial Technology for the software and resources used. I would like to specifically acknowledge Vance Green at CAST, for introducing me to photogrammetry and the ins and outs of PhotoScan and Unity game engine. A huge thankyou also, to Dr. Jason Tullis, for giving me access to the Sirius server at CAST which was used to process all the models.

A special thanks to my grandparents Jackie and Eric Lewis-leaning who bought the GoPro and Floodlight used in the project, at a time when my student budget was very tight.

This page would not be complete without also acknowledging Charla New and Kayla Sapkota for getting me into “productive” caving and cave surveying in the first place.

I owe a great deal to all of the friends, family, and teachers that have pushed and encouraged me throughout my education.

Finally, I would like to thank God as my source for everything--and for the opportunity and the ability to take on this adventure.

Table of Contents

Table of Figures

List of Tables

1. Introduction

In the age of Google Maps, GPS, and Landsat, there are few places on the planet that remain unknown. One of the final frontiers of exploration remains underneath our feet, where a small 1 by 1 meter hole in the ground may give way into a 50 meter drop, filled with glistening flowstone waterfalls, quiet pools, and unique cave adapted creatures not found anywhere else in the world. Karst features serve as a window into the subsurface, providing us the opportunity to study geology, speleogenesis, groundwater, as well as a plethora of rare, delicate, biological resources.

These discoveries, however, are not nearly as significant without a frame of reference. The first step in managing any natural resource, including caves, should be ascertaining the locations and spatial extent of that resource. In many ways the fundamental building block for all karst research is the cave survey.

From communicating the location of a colony of rare bat species to biologists, to planning the rescue of a lost or injured person, to understanding the movement of polluted water through the subsurface, and preventing the construction of highways and buildings only a few meters above structurally unsound caverns, a map is required. At the most fundamental level, cave maps are how we distinguish the passages that have been rediscovered “for the first time”, a dozen times, from the new passages and rooms where truly no person has ever set foot before.

This project will explore the way cave surveys are conducted currently, and ways they could be improved with modern technology using three dimensional models. Specifically, the research will assess the practicality of photogrammetry as a quick, inexpensive, method for the average cave survey volunteer to survey or at least document caves. The project also aims to assess the accuracy of the method in comparison to traditional methods.

1.1 Traditional Cave Survey

Currently, cave survey methods involve using manual time consuming methods. The archaic tools used, typically include a tape measure, transit compass/clinometer, and a hand drawn paper map that is later scanned into a digital format. Survey stations are set up throughout the cave within line of site of each other and the distance, azimuth, and clinometer numbers are measured between stations. Azimuth and clinometer measurements are measured from the first station to the station deeper into the cave (the front site reading), then usually double checked with a back-shot in the reverse direction. The completed network of stations with azimuths, inclinations, and distances is called a traverse. At each station along the traverse, the left, right, up, down (LRUD) measurements are taken. Distance and bearing information help the sketcher draw an accurate to-scale map of the survey line with all the survey stations. Clinometer data and floor to ceiling measurements help the sketcher to draw cross sections and profiles. Lastly, LRUD data allows the sketcher to interpretively draw in formations and passage walls in relation to the survey line. Some sketches are done only to a relative scale, but most are done to-scale on graph paper with proper orientation using a protractor.

Traditional cave survey is capable of quickly establishing survey lines which are acceptably accurate for the application. Often a Sunnto clinometer/compass is used. Some cavers also use the Disto-X, a specially modified Disto laser rangefinder upgraded to measure distance, azimuth, and inclination, all at once with the click of a button. Whatever equipment is chosen, it is likely that it is not as precise as the total stations most above ground surveyors are familiar with. Many cave surveys must be completed with handheld equipment in highly confined cave passages where the surveyor may not be able to sit up out of the prone position, much less set up a large professional tripod based total station.

Even the best surveys using these handheld tools will result in some degree of error in each shot. There are several methods of mathematically checking the survey for quality by calculating loop closure error. The survey can then be adjusted by redistributing the error evenly throughout the survey.

The fastest traverse method is called an open traverse. This is a series of survey shots with no loops and where no or only one GPS point is known. With this method mathematical checks are impossible. All other traverse methods provide the ability for a quality check to be performed.

Probably the most common method of creating a mathematically checkable survey occurs where the passage of a cave naturally creates a loop that closes on itself. Since the traverse starts at a station, progresses throughout the loop and eventually ends back at the same station, all changes in the X, Y, and Z coordinates between stations in the loop should theoretically sum to zero. This is because, at this point, the cave surveyor has moved no more north than they have south and no more east than west. (McCormac, 2004). This sum of changes will never actually be zero. If the survey data is plotted, the ends of the survey loop will not actually connect perfectly. This disparity is called the loop closure error, and is essential in determining the quality of the traverse, and its precision with respect to the total length of the survey.

It should be noted however that the ability to complete a survey loop does not require that the physical cave passage loops back on itself. Even in a completely linear passage, a survey loop can still be created by starting at the last station in the survey and beginning a new traverse in the reverse direction back to the first station, using all new stations.

A traverse does not actually even have to close geometrically for mathematical checks to be possible. In some cases where a cave or tunnel has two entrances, a linear traverse can be

mathematically closed between two known GPS points. In this case, the traverse, if plotted, will result in a final point which will not exactly match up with the second GPS coordinate. The difference between this GPS coordinate and the final coordinates calculated from the traverse represent the loop closure errors in the X, Y, and Z directions. In two dimensions, total loop closure error can be calculated with basic Pythagorean theorem (Mcormac, 2004). McCormac further indicates that in a loop with geometric closure, precision is then described by the total loop closure error divided by the perimeter of the figure created by the traverse. This idea can also be adapted into a 3D version of total loop closure error. In this case, the total closure error will be defined as $E_{closure}$, and can be calculated with the 3D version of the Pythagorean Theorem $E_{closure} = \sqrt{(E_x^2+E_y^2+E_z^2)}$, where E_x, E_y, and E_z represent the error in each coordinate direction. For traverses that do not close, perimeter can be replaced with survey length giving the equation precision= $E_{closure}$ / Survey Length.

If the precision of the survey is acceptable, and there are no obvious blunders in the data, these errors can be distributed throughout the survey to minimize their effect using several adjustment methods such as the least squares adjustment method.

The traverse method for establishing cave survey lines is a mature and effective one. However, acquiring details about the passage walls, profiles, and cross-sections is time intensive and ultimately relies on the sketcher's experience at interpreting and hand drawing the trend of the cave walls between survey stations. Because of this, a cave sketch done by two different sketchers on the same day, though similar, will never be the same. In the widely-recognized cave survey book, *On Station*, author George Dasher said that "More cave passage has been resurveyed because of poor sketch than for any other reason." (Dasher, 1994). Because of the time it takes, cross sections are typically only drawn at certain intervals or at key areas. One

final downside of free hand sketching is that the full glory of spectacular formations is typically reduced to a basic 2-dimensional symbol from the legend.

1.2 TLS vs CRP for the Creation of 3D Models

3D models created from terrestrial laser scanning (TLS) and close range photogrammetry (CRP) offer an alternative solution or at least a valuable supplement to traditional cave survey. Three dimensional scanned models are often both faster to produce than a sketch, and more informative. The models can provide cross sections anywhere, they capture unique flowstone formations and columns in the caves interior, and all this information is captured in a manner which is non-subjective, unbiased, and scientifically repeatable.

TLS is now widely recognized as a mature, reliable method to scan caves. Highly accurate LIDAR systems utilize infrared remote sensors capable of scanning hundreds of thousands to even a million points a second in total darkness. Onboard computers calculate the range to each point in the tiny fraction of a second flight time that it takes for each laser to travel to the target and back. This technology for the moment however, is incredibly expensive. Most TLS systems currently range from $20,000 for units like the Faro Focus to over $120,000 for Leica Scan Stations. Some other notable manufactures include Riegl, Trimble, and Zoller+Frohlich GmbH, all of which have multiple models of terrestrial LIDAR units suitable for scanning caves. TLS devices, besides being expensive, also often require extensive training, are too valuable and susceptible to damage to risk operating in wild cave environments, and are very limited in mobility. Most models designed by the manufactures mentioned above are tripod based units, weighing 20-40 pounds, also requiring large power sources (Idrees & Pradhan, 2016). The final products created from laser scans are accurate, but often lack color and texture quality. It should be noted however, that new developments suggest great future potential for

TLS in cave survey including newly emerging devices such as Teladynes VLP-16 “Puck”, a 100meter range LIDAR scanner that scans 300,000 points per second and weighs less than 2 pounds. The device costs $8,000, significantly less than the systems mentioned above. In 2016 Leica also released a similar handheld TLS scanner called the BLK 360. This device gathers 360,000 points per second with a range of 60 meters and only weighs 2 pounds. The BLK360 costs just under $16,000, which is much more affordable compared to most other TLS devices (Higgins,2016).

Close range photogrammetry is defined by photogrammetric operations that are conducted from less than a meter all the way up to 300 meters from the target (Mathews, 2008). “Close” in this sense is a relative term describing the short distance compared to aerial photogrammetry which commonly uses images taken at high altitudes from the scene. While CRP is a bit more challenging to work with in the total darkness of cave passages, it is cheaper, has better color resolution, and only requires equipment that is tough, waterproof, and easily transported through tight cave passages. The method is robust and versatile with the capability to work within the minimum distances of most TLS equipment. The method even be used under water where most TLS systems, besides special bathymetric LIDAR’s, fail to function. In addition to this, it takes little to no training to equip the average cave survey volunteer to acquire a set of overlapping images of a passage. Later, all that is required is one designated experienced person who has the adequate knowledge to process the photos into 3D models using photogrammetric software. It is the opinion of the author, that while the market is flooded with new highly impressive TLS designs, photogrammetry has been overlooked as a much cheaper, more practical method of basic cave survey and documentation, which is primarily conducted in harsh space-limited environments, by unpaid volunteers in their spare time.

1.3 Brief History of Photogrammetry

Since the middle to late 1800s photogrammetry has been practiced as a method of obtaining reliable information about physical objects using photographic images. In 1909 Eduard Dolezal founded the International Society for Photogrammetry (Ghosh, 1992). Later on, in response to the first two world wars, photogrammetry rapidly developed as a reconnaissance tool. Photogrammetry began as more along the lines of what we would think of as "aerial image analysis", using stereographic aerial imagery spread apart on a page to create a parallax. With specialized stereogram glasses, this provided the ability to view landscapes and objects in the flat image in 3D. During WWII, this allowed image analysts to detect rocket sites and other military structures which were not as apparent in 2D photographs (Howard and Rogers, 2012). After the war, civilian applications developed in geological surveys, mapping, and forestry. In the 1970s, photogrammetry shifted away from physical hard copy photographs towards processing digital images on a computer screen (Cooper, 1998). Soft copy photogrammetry, as it is now called today, has progressed to the point where we are now able to make fully 3 dimensional models on a computer simply by processing a collection of overlapping digital images.

In the past, it was critical that soft copy photogrammetrists use metric cameras and avoid moving light sources, shadows in the imagery, and off-nadir shots (Matthews 2008). While these are still good guidelines to follow, the technology has evolved to the point where many of these limitations are no longer strict requirements. Additionally, proper image matching and scaling in traditional soft copy photogrammetry required the use of specialized scale frames and networks of carefully pre-placed and pre-surveyed photogrammetric target control points. (Westoby, Brasington, Glasser, Hambrey, & Reynolds, 2012).

These targets had to be manually identified in photos along with other common points in the images to facilitate the "re-sectioning" process, where camera positions and orientations are calculated. (Westoby, et al. 2012). Alternatively, if control points were not set up, every camera pose and position had to be measured and known as the photos were taken. (Westoby, et al. 2012).

Today with advances in the technology including the development of structure-from motion (SfM) methods, no control information of any kind is required to construct a photogrammetric model. This method uses a highly redundant self-calibrating bundle adjustment to approximate image positions and scene geometry automatically and simultaneously, simply from the overlapping image pairs (Westoby, et al. 2012).

Rather than manually creating and selecting control targets and other common points within the input photographs, the software automatically identifies and matches thousands of common points, termed "key points" in the input photos. These key points are identified and grouped into features through the use of object recognition algorithms such as the Scale Invariant Feature Transform (SIFT) operator created by Dr. David G. Lowe. SIFT uses identified key points to extract features which are "invariant to image scaling and rotation and partially invariant to changes in illumination and 3D camera view point" (Lingua, Marenchino, & Nex, 2009).

Using SIFT or several other similar algorithms, the key points are linked and encoded as tracks. Tracks relate the 3D coordinates of a point in the scene to the corresponding 2D coordinates in the input images. The aligned photos are then used to estimate camera pose, then target object geometry is calculated to produce point cloud layout of the three-dimensional scene (Furukawa, 2013).

Although this process is much faster and less tedious, models derived from the SfM approach at first lack scale and orientation. While they may be correct within the relative "image space" coordinate system of the model, for many applications the next step is to align this image space to a real-world object-space coordinate system using a 3D similarity transformation (Westoby 2012). To transform the model from the relative space to an absolute coordinate system there must be at least three recognizable points in the model, of which precise real world coordinates are known. This can be done post hoc, by surveying distinct natural objects in the scene, or a priori using a small network of high contrast control targets.

1.4 Overview of Cave Survey Accuracy Standards

A major goal of this project will be to assess the accuracy of photogrammetry as a survey method. To make any claim that the proposed method has or does not have "acceptable accuracy", it is important to first investigate what the currently held standards and expectations for cave surveys are. Traditional surveys have been conducted much the same way for the past 60 years. A bulletin from the 1962 National Speleological Society states that a transit and steel tape survey should have all points within a circle of error with a radius of 0.14% as long as the survey line. (Schwinge, 1962). For a 1000 meter survey, that leaves an acceptable loop closure error of 1.4 meters at most. Modern cave survey standards in the United States tend to be vague and vary largely upon the specifications for the survey given by the cave owner. As an American system has not yet been created, often a widely-recognized survey grading system created by the British Cave Research Association is used as a framework to evaluate the quality of survey products. The hierarchical BCRA system is illustrated in tables 1 and 2 on the next page.

The accuracy of these surveys hinges on the precise reading of angles with as little error as possible. Many attempts have been made to assess the accuracy of cave survey techniques over the years but this is often a difficult question to answer because there is no perfect control with which to compare to. Much of the literature concerned with assessing cave survey accuracy is not totally conclusive and simply presents a statistical analysis of standard deviation and other measures of central tendency for survey loop closure adjustments. (Thrun, 2009). However, in a recent study of the accuracy of a large collection of surveys conducted in West Virginia, it was found that no survey met the BCRA grade 5 standards (Thrun, 2009).

Accuracy, as described in this paper, will be defined as a measure of how close a position or measurement is to its true value. This should not be confused with precision, which refers to the closeness of results to each other with regards to repeated attempts to measure the same position or distance. It should also be noted that there are different types of accuracy and errors in the realm of geospatial science and cave surveying. A model must first be evaluated based on its relative or "point to point" accuracy within the image space. This type of accuracy is concerned with comparing the distance between two or more recognizable points in the virtual model versus the same distance between those points in real life ("Positional Accuracy," 2003).

Relative accuracy can also be used to assess the difference between a point cloud model generated through the use two different methods such as TLS and photogrammetry. In this case relative differences between the point clouds can be described through the Hausdorf Distance. The Hausdorf Distance measures the degree of mismatch between two point clouds by taking each point in the first point cloud and finding the point that is furthest away from it in the second point cloud and vice versa the in opposite direction. The maximum distance between any point in the first point cloud from any point in the second cloud is then said to be the Hausdorf

Distance. (Huttenlocher, Klanderman, & Rucklidge, 1993). The results of this operation cannot determine whether a method is "more" or "less" accurate than another, but can determine how much the model or point cloud deviates from another which is generally assumed to be more accurate.

To the contrary, absolute accuracy is a measure of how accurately an object is positioned with respect to its true position in an absolute reference frame. For this type of accuracy assessment to occur, the relative image space coordinate system must be aligned to a real-world coordinate system using a 3D similarity transformation. ("Positional Accuracy," 2003).

Just as there are different kinds of accuracy, there are also different types of errors. Systematic error is error which has a non-zero mean. It is constantly biased by the same amount in one direction and accumulates over time. An example would be an uncalibrated Suunto compass transit which always shoots 1 degree off in a specific direction. Systematic errors start off small and negligible for small surveys but become enormous on long surveys (Thrun, 2009). Fortunately, if the cause of the error can be recognized, it is often very easy to fix. Random error on the other hand, consists of small errors in measurements which are not biased to a direction and are directly related to the precision limitations of the measurement instrument. All measurements besides counting have some degree of random error. (Thrun, 2009). If these errors are small, they tend to balance out over a survey and can be modeled with a normal (Gaussian) curve. (Thrun, 2009). The most important kind of error to avoid in cave survey is large random errors called "blunders." Writing down a number incorrectly, or reading the wrong side of a clinometer, among several other things can cause serious blunders that can drastically throw off a survey.

Table 1 BCRA Accuracy Standards for Survey Line	
Grade 1	Sketch of low accuracy where no measurements have been made.
Grade 2	May be used, if necessary, to describe a sketch that is intermediate in accuracy between Grade 1 & 3.
Grade 3	A rough magnetic survey. Horizontal & vertical angles measured to ±2.5º; distances measured to ±50 cm; station position error less than 50cm.
Grade 4	May be used, if necessary, to describe a survey that fails to attain all the requirements of Grade 5 but is more accurate than a Grade 3 survey.
Grade 5	A Magnetic survey. Horizontal and vertical angles measured to ±1º; distances should be observed and recorded to the nearest centimeter and station positions identified to less than 10cm.
Grade 6	A magnetic survey that is more accurate than grade 5. A Grade 6 survey requires the compass to be used at the limit of possible accuracy, i.e. accurate to ±0.5º; clinometer readings must be to the same accuracy. Station position error must be less than ±2.5 cm, which will require the use of tripods at all stations or other fixed station markers.
Grade X	A survey that is based primarily on the use of a theodolite or total station instead of a compass, (see notes 6 and 10 below) A Grade X survey must include on the drawing notes descriptions of the instruments and techniques used, together with an estimate of the probable accuracy of the survey compared with Grade 3, 5 or 6 surveys.

Table 2 BCRA Accuracy Standards for Cave Passage Detail	
Class A	All passage details based on memory.
Class B	Passage details estimated and recorded in the cave.
Class C	Measurements of detail made at survey stations only.
Class D	Measurements of detail made at survey stations and wherever else needed to show significant changes in passage dimensions.

1.5 Study Area

This study takes place in several caves throughout the Ozark Plateau Region in Northern Arkansas. This region is dominated by limestone and dolomite formations, chiefly the karstic Boone formation which consists of interbedded limestone and chert. It is the presence of this thick carbonate formation which facilitates karst development, hosting 78% of the caves found in the Buffalo River National Park. (Hudson, Turner, & Bitting, 2011).

The first experimental pilot study took place in a small cave located in Bentonville, AR. This cave provided an opportunity to conduct the very first cave experiment and determine whether the idea of using photographic images from a GoPro camera to model a cave would work at all. Two trips were made to this cave which worked as an initial testing ground for various hardware and software methods and settings.

The next part of the study took place in Searcy County, AR where the method was utilized in a cave with much larger rooms and passages. This cave has an interesting history and is so large that it was surveyed by the Department of Defense with intentions of using it as a possible nuclear fallout shelter. This part of the work focused on the limits of the proposed

system which was used to scan large passages and rooms over a 30 meters wide. Experiments were also conducted here attempting to capture high resolution models of individual cave formations and integrate them back into the larger model. This cave also provided a good test for using survey traverse data to calculate GPS coordinates for control targets deep in caves where satellite reception is not possible.

Additional research was conducted in two caves in the Buffalo National River area with permission from the National Parks Service and the support of volunteers from the Cave Research Foundation. This part of the research focused on demonstrating the quick ease of use and positive results of the method in the average small-to mediums sized caves that are common throughout the park.

Lastly, a final field project was conducted in the University of Arkansas utility tunnels. The manmade structure offered a chance to spot any obvious distortion from the fish eye lens that would not be as apparent in natural abstract structures such as the previously studied caves**.**

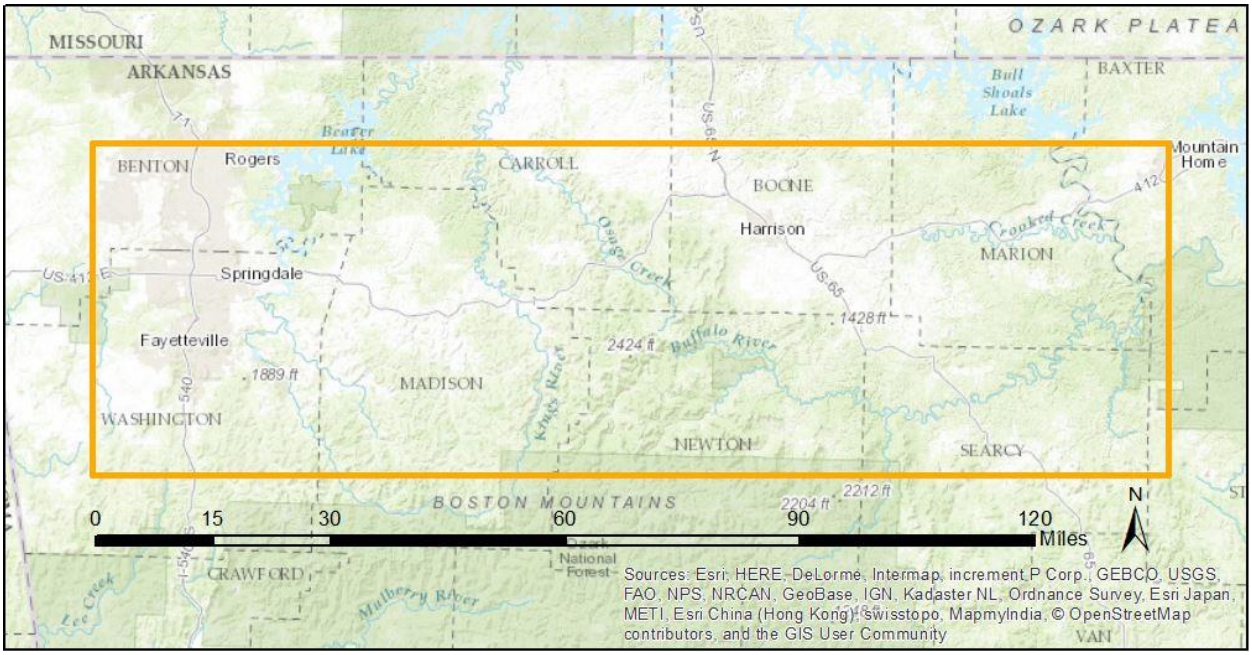

Fig 1. Study Area

2. Literature Review

A large body of research exists that describes the use of TLS systems as a method to survey caves. There are also abundant instances where photogrammetry has been integrated with TLS for cave survey. Outside of cave survey, photogrammetry is often used as a stand-alone method for many applications, as well as being integrated with TLS for finished products. However, there has been only sparse research experimenting with the use of photogrammetry as a completely independent low cost means for basic cave survey and documentation.

2.1 TLS for Cave Survey

The following list of works is in no way meant to be exhaustive as there has been an enormous amount of research into using TLS for cave survey.

One of the first attempts on record began in 1988 where researchers used one of the first TLS scanners, the Minolta VI scanner, to model Altamira Cave in Cantabria, Spain. The project took over 10 years to complete due to the difficulty of using the scanner which had only about a meter range, and a large amount of the work that had to be done manually (Idrees & Pradhan, 2016).

About decade later in 1999, a group of researchers out of the United Kingdom used an automated TLS system designed by Measurement Devices Limited to survey the rock shelter of Cap Blanc in southwest France. This Autoscanning Laser System (ALS) consisted of a tripod with an automated rotating mount carrying a Leica Disto laser range finder. The team completed two scans of the rock shelter which had a resolution of 2cm (Brown, Chalmers, Saigol, Green, & D'errico, 2001).

One of the first TLS cave mapping projects to be conducted in the U.S was at Chapel's cave in southwestern Oregon. This project used the Cyrax 2400 scanner and is one of the first projects that tested the feasibility of TLS for cave survey. After the model was created, highly accurate horizontal and vertical cross-sections were extracted. (Idrees & Pradhan, 2016).

Moving forward, more TLS survey research was published in 2009 regarding work done in Wonderwork Cave, which represents one of the only TLS cave scans conducted in Africa. Wonderwork cave is a very large dolomite solution cavity located in the Northern Cape Province of South Africa. The cave was scanned with a Leica HDS 3000 primarily to set up a framework for archaeological research at the site. The scan took only three days of field work and comprehensively mapped all the cave walls and excavation sites. (Rüther, et al., 2009).

Also published in 2009, was a project which used a Riegl LMS-Z420I to model Dachstein South Face cave in Austria. This research was distinct in that, instead of a historical preservation motivation, it focused on studying water storage capacity of the cavities and structural geology of the mountain. Another distinguishing feature was the more extreme and wild nature of the cave. While TLS surveys are typically done in easier horizontal "walk-through" caves, this project pioneered laser scanning in complex partially vertical survey environments. Part of the logistics included transporting the scanner through tight spaces as well as with researchers down a 60-meter rappel all with dripping water from overhead (Buchroithner & Gaisecker, 2009).

Two years later, another team in Austria studied Marchnhohle cave using the z+f Imager 5006i terrestrial laser scanner to create very high resolution (1.66mm) scans of the cave. These scans were significant to studying speleogensis and micro to macro cave morphology features

that are not normally recorded in a traditional cave survey (Roncat, Dublyansky, SpöTl, & Dorninger, 2011).

Also published in 2011 is work by Aaron Addison in the historic longest cave system in the world--Mammoth Cave in Kentucky. Addison successfully scanned a 4km section of the cave merging 135 different point clouds made up of a total of 18 million data points. The point cloud was later reduced to 500,000 points for visualization as most software currently cannot handle such a large dataset. As a part of the discussion of the research, several limitations were mentioned regarding using laser scanning in the cave. It was noted that the project was difficult to complete due to the high humidity which caused condensation on the equipment, thermal gradient from the airflow into the cave causing out of range values for the temperature compensators on the device, sand and rock fragments getting into mechanical components such as tripod legs and mounting instruments, as well as the normal hazards of equipment getting dropped and broken in the wild cave environment. Addison also discussed the issues with getting the scanner to scan large vertical sections in mammoth dome where the scanner had difficulty sighting the high angle survey stations. Lastly, Addison mentions the limited mobility of the system which weighs 18kg and is a highly fragile sensor. The project was completed using the readily available power supply along the caves tour trail, but had this not been available, the device would have required two 12-volt auto type batteries to power it, exacerbating the weight and logistical awkwardness of transporting the already cumbersome equipment. Despite the limitations this research went far in proving the maturity of TLS and its feasibility for scanning very long cave systems (Addison, 2011).

Research published in 2012, discusses the use of a FARO Photon 20/120 to scan Eisriesenwelt the largest ice cave in the world. Due to global warming, the ice is beginning to

melt in the cave. While there is some intrinsic value in preserving the landmark, it also serves as an important tourist attraction, drawing around 150,000 people a year to journey through the 42 kilometers of tangled icy corridors and massive halls. The "World of Ice Giants" as it is also called was scanned to quantify the amount of existing surface ice to be used as a baseline to monitor future ice loss. The research also has the potential to identify areas prone to hazard. Lastly, a complete fly through of the cave captured the amazing icy cavern for posterity (Milius & Petters, 2012).

2.2 Integration of TLS and CRP for Cave Survey

It is widely recognized that both TLS and CRP have their advantages and disadvantages. As such, there is a large body of research discussing the integration of the color and texture quality of photogrammetry with the accuracy of TLS for photorealistic cave surveys.

A project that first pioneered this idea occurred Baiame Cave in New South Wales, Australia. The work, which was published in 2004, developed a workflow for creating a high resolution realistic model through the combined us of a Riegl LMS-Z210i scanner and an inexpensive Nikon coolpix digital camera. For this project, control points were first surveyed with a total station and used to automatically register the texture information from the photogrammetry to the accurate 3D geometry of the laser scan. While the scans were taken in Australia at the site, they were processed independently by a team in Canada. The final model of the cave and its various aboriginal rock art and cave paintings were captured for posterity as well as research on prehistoric living (El-Hakim, Fryer, & Picard, 2004).

A very similar workflow was used in 2009 in two caves in Spain: Las Caldas and Peña de Candamo. This was one of the first of many 3D cave modeling projects that would be conducted in Spain. This research utilized the same multi sensor approach where control points where first

surveyed with a total station and then used to combine scans from a Trimble GS200 scanner with images from several digital cameras. This research used convergent images taken with the traditional rules of photogrammetry, independent high resolution close-up images of the cave texture, and panoramic images using a fish eye lens to provide 360 degree panoramic images of the cave. The method used in the Spanish caves was particularly useful for capturing the abundant delicate Paleolithic art forms—but the researchers also recognized the potential use for studying cave morphology and speleogensis. The authors also discuss future possibility for improvement with the software utilizing the Scale Invariant Feature Transform (SIFT) algorithm (González-Aguilera, Muñoz-Nieto, Gómez-Lahoz, Herrero-Pascual, & Gutierrez-Alonso, 2009).

In 2010, also in Spain, Parpalló Cave was scanned using a joint photogrammetric and TLS process. This cave is one of the oldest known and most important international world heritage sites. The laser scan data was acquired with a FARO LS 880HE scanner with a range of 75 m and a resolution of up to 3mm. This point cloud was registered with the photogrammetric point cloud using artificial white spherical targets provided by the manufacturer. This greatly improved on the existing 2D hand drawn sketch which was later determined to have poor metric accuracy when compared with the data from the TLS survey (Lerma, Navarro, Cabrelles, & Villaverde, 2010).

In the same year, research was published regarding the modeling of the Bronze Age Cave Les Fraux in Perigord, France. The cave is one of the most studied caves in Europe containing numerous artifacts and engravings. This team used a network of reference GPS points outside the cave, along with surveyed spheres and coded targets to register the photogrammetric model with the TLS model. A FARO Photon 80 and 120 were used for the laser scan, and a Canon EOS 5D with 28 and 85 mm lenses was the primary camera for acquiring images for the photogrammetric

model. This camera was equipped with a flash ring to collect imagery in the darker parts of the cave. For this project, texturing had to be conducted manually as an automated method of identifying corresponding points in the images was not yet readily available (Grussenmeyer, Landes, Alby, & Carozza, 2010).

A similar approach to the above examples was used in research published in 2011 discussing the modeling of two more Spanish caves Buxu Cave, and La Loja cave. These two caves were surveyed using a Nikon D80 Camera, Canon 500D, and a Trimble GX. The authors of the paper emphasized the importance of cataloguing Paleolithic art and integrating them in a GIS for better management. The authors also discussed the advantages of capturing these places and presenting them virtually for the many people with disabilities who cannot visit the caves themselves (Gonzalez-Aguilera et al., 2011).

In 2013 more research was published at another Spanish location, Can Sadurní cave. For the Can Sadurní project, control targets were first surveyed with a Leica TCR 705 total station. After this, large scale structures such as storage silos and a combustion structure were surveyed using photogrammetry. The cave itself was scanned with a Reigel 420i sensor and combined with texture information from photographic images to create a photorealistic model. The team noted the difficulty of acquiring images with good radiometric quality and suggested that a structured light system could resolve the problem in future research. The project successfully created a spatial frame with which to incorporate with a GIS for continued archeological excavation. The model also helped in analyzing the stratigraphy of the cave and the gradual process of sedimentation that infilled the cave (Núñez, Buill, & Edo, 2013).

Another study done in 2013 studied the Gomantong caves in Malaysia. The Gomontong caves are comprised of two caves Simed Hitam (Black Cave) and Simid Puteh (White Cave).

Because the publically available ASTER digital elevation model had pretty low spatial resolution, the researchers used aerial drone based photogrammetry on a Gate Wing X100 UAV to model the mountain side containing the caves. After this was complete, a Faro Focus 3D scanner was used to scan the caves. The model took 69 scans and produced over 5 billion data points. The model was integrated with traditional cave survey techniques to create highly accurate plan view surveys of the caves. It was also useful for establishing volume densities for the caves, and establishing the greater volume density in Simed Hitam. Researchers were interested in why there was such a large difference in volume densities for the caves, as Simed Hitam has a much higher volume density than what would be expected from natural hydrologic processes. It is believed that the biology of each cave played a significant role in the differing morphologies of the caves, as Simed Hitam has much larger swift and bat populations. The activities of these animals as well as the increased amount of guano may have played a part in quicker erosion and weathering of the cavity. Additionally, researchers noted that the scan was such good resolution that individual animals and nests could be identified. The authors hope to develop an automatic algorithm in the future that automatically acquires bio inventory count data by species (McFarlane et al., 2013).

2.3 CRP and TLS for applications outside of Cave Survey

Photogrammetry has been used by itself for cultural heritage preservation for many years. One such example was research published in 2005 were researchers photogrammetrically modeled aboriginal pictographs and petroglyphs. This was especially useful for capturing the pictographs as they represent art that is painted onto a 3-dimensional rock surface, not a flat planar surface. Furthermore, the research proved that the operation could be conducted with

satisfactory results using nothing but a cheap Nikon Coolpix 3100 three-megapixel camera (Chandler & Fryer, 2005).

Other interesting uses for photogrammetry include modeling steep mountain terrain. This idea was mentioned in 2011 by N. Kolecka. This research project involved modeling the steep western slopes of the Kóscielec Mountain with a Nikon D80 SLR 10 MP camera. The photogrammetry was compared to a TLS which were found to have similar results. The final product demonstrated the significance of photogrammetrically derived digital terrain models in creating detailed representations of the steep rock faces to be utilized for planning rock climbing routes. The author also discusses potential uses in tourism, engineering, geomorphology, and studying rock fall and avalanche hazards (Kolecka, 2011).

Another alternative use for photogrammetry is in modeling historical architecture. One example would be the Beufort Castle in Lebanon, where researchers tied together several hundred photos from a variety of cameras to model the castle. Some of the images were oblique photos taken by helicopter using the CIPA 3x3 rules as a guideline. The result of the project was a 3D virtual re-creation of part of the castle, created from both modern and historical images that included parts that are now destroyed or buried (Grussenmeyer & Jasmine, 2003).

Similar work was published a year later by the same author, concerning several more case studies in France such as modeling the Gallo-Roman Theatre of Mandeure using a combination of TLS and dense stereo image matching as well as Engelbourg Castle with a similar methodology. In the discussion of these two projects the authors said the slow scanning speed and small field of view of the Trimble GX TLS made it not suitable for covering the large study site. The 2-meter minimum scanning distance also added limitations for scanning between

some of the dense collections of ruined buildings. The TLS point cloud was then completed by integrating it with a photogrammetric one (Grussenmeyer et al., 2012).

Recently, in 2014, Yang Liu and Julian Kang from Texas A&M University experimented with photogrammetry as completely independent method of surveying the interior of buildings. They divided the first floor of the target building into 20 sections which were scanned with a Canon EOS Rebel T3I SLR camera mounted to a tripod with a panoramic head. Sticky notes were used to efficiently image the rooms with the right amount of overlap between photos. The researchers found that the model had an average difference of -.43% in comparison to the CAD drawing provided by the University. The final results portrayed the features of the interior of the building very well and at an acceptable level of accuracy considering the low budget nature of the research, and that TLS was not used.

2.4 CRP as Standalone Method for Cave Survey

In Le Grotte De Castellana Spain, researchers tested both the TLS method, and an independent photogrammetric method with a Nikon D100 camera and found that both methods had pros and cons—the TLS method had more accurate geometry, while the photogrammetry had better color and texture resolution (Caprioli, Minchilli, Scognamiglioi, & Strisciuglio, 2003).

A couple of the same researchers who mapped Baime cave in 2004, as mentioned in the previous chapter on integrated TLS and CRP surveys, also went back and mapped the same cave a year later to experiment with using photogrammetry alone to model the cave. The researcher's first surveyed photogrammetric targets with a total station then used a 6 Megapixel Kodak DCS460 and a 3 Mega pixel Nikon Coolpix camera for image capture. The images were then processed in Leica Photogrammetry Suite. The authors noted that by using the digital cameras alone, much of the field work logistics were made easier as they didn't need to carry the

previously used bulky scanner and its power supply. The main concern for digital image correlation in the project was whether there would be enough texture on the surface for automatic generation of the key points. This remains an issue for using photogrammetry as a stand-alone method in caves with homogenous wall texture and geometry. Overall, no firm conclusions could be drawn as to which method better characterized the cave (Fryer 2005).

Recently in 2012 another low budget, photogrammetry project was conducted in El Niño Cave in Spain. The researchers used a Nikon D90 to model a panel section of a cave with numerous Paleolithic paintings mostly of animals. While the final results were not quite as accurate as a laser scan, the authors felt that the product appropriately accomplished the needs of the project to document and archive the rock art (Moreno & Garate, 2012).

3. Statement of the Problem

Cave survey is vitally important to karst science and management. Yet while survey methods have evolved rapidly above ground, cave survey remains much the same. Hand drawn surveys take time, skill, and are limited in what they can capture and how precisely they can capture it. 3D modeling using LIDAR scanners offers a whole new way of capturing entire environments with great detail and accuracy, but also brings its own set of challenges. If traditional survey seems archaic, LIDAR can seem rather impractical and "over the top." While LIDAR could be the way of the future, it currently involves the use of incredibly bulky and expensive devices that are not built to work in confined passages, or when partially submerged in mud and water. While large tour caves are currently being scanned with TLS systems, this methodology is not yet practical for the average cave survey volunteer in the average cave. Advances in digital photogrammetry offer the opportunity to study a new method of obtaining 3-dimensional cave models. The methodology discussed in this paper is designed to improve on

the limited capabilities of traditional survey, and provide similar results to laser scanning, while using equipment that is inexpensive, rugged, and easy to use. This thesis project will test and evaluate the use of fisheye lens photogrammetry as a survey method in caves, a research area that is not well documented in the fields of photogrammetric and karst science.

3.1 Research Questions

Two major research questions will be addressed. Firstly, under what if any conditions can pure stand-alone photogrammetry be used to create interpretable 3D models of interior cave structures? There must be an emphasis on the word interpretable here, as it is likely that almost any set of related overlapping images will produce something in Photoscan. In this case, successful interpretable models should be largely complete, aesthetically attractive, and must correctly represent the environment in such a way that the viewer can understand the general layout of the cave. The study will explore the effects of cave size, water, and mazy or sinuous caves on the quality of the finished model. Various capture methods, camera settings, and processing parameters will also be explored.

A secondary question will be to establish whether or not models created using the proposed method are acceptably accurate with respect to the application of cave survey, and compared to the currently held standards and expectations for traditional cave survey. Part of answering this question will involve comparing 2D maps derived from photogrammetry to traditional survey maps. After models are georeferenced, real world measurements will be compared to measurements in the virtual model. Finally, the error values in the PhotoScan processing reports of each model with be evaluated to determine the precision of both the photogrammetric method, and any control networks used to georeferenced the models.

4. Materials and Methods

4.1 Study Design

The first objective of this study was to ascertain under what if any conditions can pure photogrammetry be used to create useful interpretable 3D models of cave structures. For this research to occur, there was first a brief study of the photogrammetric process in general. After this study was complete a very rough experiment was conducted to provide a "proof of concept" and see if overlapping images from a GoPro camera taken in a dark cave would in fact create a model at all. While the first attempt failed, modifications were made to the software, hardware, and methodology until the first successful cave model was produced. Gradually, this methodology was tweaked and tested in several different caves of varying sizes and characteristics. These caves were given the aliases "Aspen", "Birch", "Cedar", and "Dogwood" to protect their true names and locations.

Photogrammetry was chosen over other cheap 3D modeling techniques such as using a modified Xbox Kinnect for several reasons. The GoPro is both more portable and more rugged than the modified Xbox Kinnect system which is not waterproof and requires being connected to a laptop computer during its operation. Photogrammetry also allowed for the creation of full color textured models as opposed to the often-lower quality color and texture information in models from the Kinnect's RGB camera. Photogrammetry also uses regular images, without any changes to the programming of the GoPro Camera. Google Tango was also briefly considered, but was dismissed do to its limitations in only being available on a few android phone and tablet models.

While Autodesk 360 Recap was used in the first experiments, Agisoft PhotoScan quickly became the software package of choice for the project. 360 Recap from Autodesk, offered an

initial user-friendly method of making photogrammetric models from input photos, but was essentially a "black box" with very few options for controlling how the images were aligned and processed. PhotoScan allowed for camera based calibration, complete control over every step in the processing, a wide variety of post processing tools, the ability to georeference models and export them to a wide variety of formats, and the ability to process the data in "chunks." PhotoScan was also chosen over Pix4D, from Pix4D Inc., due to the substantial price difference, as well as PhotoScan's reputation for being better used for convergent photogrammetry as opposed to the parallel stereo photogrammetry that Pix4D excels at.

The camera chosen for the project was a GoPro camera which has a wide angle fisheye lens. While this camera inevitably creates more distortion than a conventional camera with a standard lens, it also allows for the simultaneous capture of cave floor, left and right walls, and ceiling all at once with a large amount of overlap between photos. Conventional cameras excel at modeling a wall, or a ceiling, or the ground, and when pointed directly perpendicular to these targets can provide highly accurate measurements. However, these cameras require a much higher quantity of photos to achieve the overlap required to model a tunnel or cave passage environment. It is likely that the nature of the wide angel fisheye lens, as well as the relatively new support added for this style of lens in software like PhotoScan, is what made this project possible (Higgins, 2015).

Initial tests used a bright helmet mounted headlamp but it was quickly realized that an even brighter light was needed. There are many bright spotlights on the market, but instead a floodlight was chosen so that the large amount of light would be spread evenly across the environment instead of being concentrated in one area. A water-resistant portable rechargeable floodlight was chosen so that it could be used in cave environments.

While the successful construction of several cave models was exciting, it was important to ensure that such models were easy to manipulate, navigate, explore, and share with others effectively. Several end products were tested such as interactive 3D PDFs, Unity Game Engine (Unity Technologies) models, Fly throughs and rotating models generated with ESRI's ArcScene, as well as more classic 2D maps based on the X-Y extent of the model. Viewing of the models in virtual reality was also considered but was not pursued in this project.

The secondary objective of the research was to examine the meaningful quantitative information that could be retrieved out of georeferenced models and assess the accuracy of that information. Obtaining GPS coordinates for ground control points presented a new challenge in cave environments which have no satellite signal. The term "GPS" is used in this paper in the place of the more correct term "GNSS" due to its more widespread familiarity among cavers and karst scientists. Two different methods were developed for georeferencing the models. The first, a quick and dirty method for small caves, involved simply surveying three control targets around the entrance area of the cave. The second method was more intensive involving the use of trigonometry and cave survey line traverse data to calculate the coordinates of control targets throughout the cave.

An additional challenge was found in attempting to assess the accuracy of cave models and how closely they represented the true cave. To do this, measurements in the model were compared to real life in-cave measurements. 2D maps were also extracted from the model and compared with cave survey maps constructed with traditional survey methodology. While these products were similar, it was hard to say that either one was more correct than the other, or that either one accurately represented the highly abstract shape and structure of the caves. Unfortunately a LIDAR unit could not be acquired to compare the photogrammetric point cloud

to a TLS point cloud. So that any distortion from the fisheye lens would be more recognizable, the method was also utilized in manmade tunnel.

4.2 Image Acquisition

The method used to acquire images of cave passages was non-invasive involving the use of a simple "survey rig" which consisted of a GoProHero3+ Black Edition camera securely mounted to a 1000 lumen Husky cordless rechargeable floodlight, with an attached Iphone 6 connected to the GoPro via Wi-Fi. A GoPro handlebar mount was used to attach the GoPro to the floodlight, while Velcro command strips secured the iPhone 6 to the back of the floodlight. This survey rig was a vast improvement over the initial experiments which used only a GoPro and Princeton Apex headlamp mounted to a caving helmet.

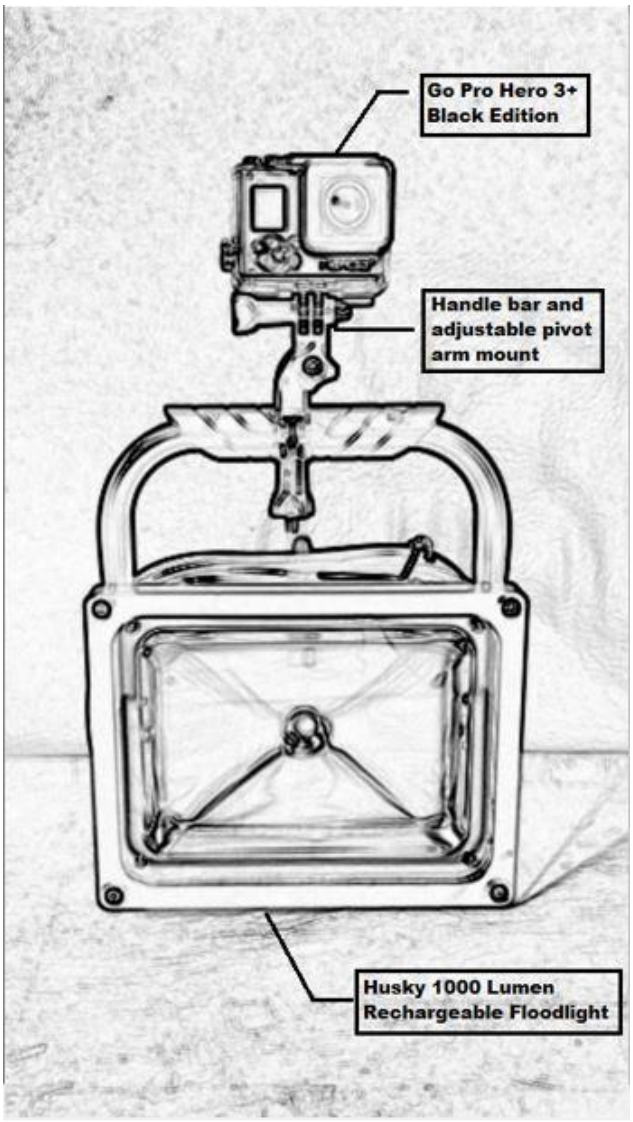

Fig 2. GoPro Survey Rig

The Husky rechargeable floodlight was chosen due to its inexpensive price ($50), tough waterproof resistant housing, cordless portable nature, as well as its ability to illuminate cave passages far better and more evenly than spotlights of similar brightness. The floodlight was able to produce 1000lumens for about 3 hours, which was far longer than necessary to take the images of each cave.

The Iphone 6 was cased in a LifeProof case and mounted to the back of the floodlight for live feedback to make sure images were clear and consistent overlap was achieved between shots. Live feedback and camera settings were controlled on the iPhone using GoPros "capture" app via a WiFi connection with the camera.

The camera used throughout the project was the GoProHero3+Black edition. This was a relatively inexpensive camera purchased for around $350. According to GoPro's website, when shot on 12MP wide setting, the camera has a 122.6 degree field of view ("Hero3+ Black Edition Field of View Information"). The EXIF data from the camera indicates that it has an estimated 3mm focal length, which can be viewed as roughly equivalent to a 17.2 mm lens on a 35mm

camera. The cameras aperture (f-stop) is fixed at f/2.8. Lastly, ISO and exposure time (shutter speed) settings are variable and automatically controlled for the best results by the camera.

Some obvious advantages to this camera, besides the price, include the easy mounting options which allowed for its attachment to the floodlight, as well as the extreme ruggedness of the device. This camera, while attached to the survey rig, was easily fit through tight spaces, smacked against rocks, and pulled through muddy cave passages with little concern. The camera is fitted with a wide angle fisheye lens which brought both pros and cons. There is undoubtedly greater distortion using a fisheye lens especially around the edges of each photos compared to the lenses found in more traditional DSLR (digital single-lens reflex camera.) However, the 12MP resolution, coupled with PhotoScan's automatic camera calibration technology, largely mitigated the effects of this distortion. The upside of this lens was its ability to capture more of the environment with each individual image, allowing for better image overlap and more information about how objects in the scene are connected. While DSLR style cameras work well for capturing a wall or ceiling by itself, the wide-angle fisheye lens was chosen for its advantages in capturing entire "tunnel" environments where it can gather information on the floor, left wall, right wall, and ceiling all simultaneously without ever directly looking at any of them. While it may be possible achieve similar tunnel photogrammetry models with a DSLR camera, it would most likely take a great deal more photos and would likely be far more challenging to perform image matching on the larger set of photos taken with the sensor pointed in widely varying directions (Higgins, 2015).

The fixed f-stop of the camera was also an advantage in that it insured that the aperture size remained consistent throughout the data collection. Keeping the sensor size constant is an important photogrammetric rule of thumb. While the maximum limit of the ISO

setting can be adjusted, the both ISO setting and the shutter speed are automatically controlled by the camera to achieve the most optimal results. While it would be nice if these settings could be manually controlled, the automatically chosen settings worked well for the purposes of this system which was designed to be used by the average cave survey volunteer who may or may not have extensive photography knowledge.

It should be noted that there was some experimentation with both time lapse photography which allowed for the automatic capture of photos every few seconds, as well as the use of video walk throughs of caves. Videos were split into hundreds of individual frames which allowed for an extremely quick capture of long passages with guaranteed overlap between frames. This video methodology was proven valid as a quick and method of data capture which sacrificed quality for speed.

The primary image capture setting in this research however, was the 12MP wide single photo method which took more time, but resulted in higher quality images and models.

The capture procedure used was highly unconventional in comparison to traditional photogrammetry where camera shots are always taken perpendicular to the target and a moving light source is never used. As it would be impractical to scan the left wall, right wall, ceiling, and floor, independently, and furthermore improbable that the software could recognize and tie the four scans taken at right angles to each other together, this study approached the problem a different way. For all the models created in this research the GoPro was transported largely parallel to its targets, progressing down the center of passages to acquire depth information by moving through the area. This procedure does not fit into either the parallel or convergent classifications for traditional stereo photogrammetry. This idea combines structure from motion (SfM) methodology with Simultaneous Localization and Mapping (SLAM), a computer vision

concept largely studied in autonomous robotics and self-driving cars (Urban & Hinz, 2016). The idea is very similar to the way humans process the dimensions of a hallway and localize themselves and their progress as they move through it. While the wide-angle fisheye lens introduces some distortion, it also better facilitates the SfM SLAM photogrammetry approach allowing the camera to have some limited peripheral view of the walls, ceiling, and floor, all while remaining pointed in the forward direction down the center line of the passage.

Some experimentation occurred with taking side shots and ceiling facing shots with little success. A method of capturing large rooms was attempted by walking around the perimeter of the room while facing the camera such that it was pointed at an imaginary object in the center of the room. This technique was also not very successful, probably due to the challenge of getting the light to reach the other side of the room. For cave formations and other points of interest in cave models, like columns, images were taken from all angles of the feature which was processed as its own "chunk" and then integrated with the larger model. The utilization of "chunks" is further discussed below.

4.3 Model Construction

Initial experiments used Autodesk 360 Recap which is a simple free online software program which allows users to upload images to the website to be processed into models. This worked great for the first few tries but was essentially a "black box" in that there was no control over how the model was processed. Due to the highly-limited nature of 360 Recap, PhotoScan was quickly adopted as the software of choice for model construction. The PhotoScan software can be purchased at anywhere from $59-179 for the standard version, and $549-$3,499 for the professional version. While the standard version is all that is needed to simply create cave

models, the professional version is required for more advanced functions such as the use of control points to create georeferenced 3D models and orthomosaics.

All models were processed using PhotoScan version 1.2.3 except for the utility tunnel models which were processed in version 1.2.6. Finished models were later viewed in versions 1.2.6 and 1.3 so that more recently developed features such as the ruler measuring tool could be utilized. Created by the Russian company Agisoft, PhotoScan offers an interactive software program which allows the user to control every aspect of each step in the processing. PhotoScan stood out over other software such as Pix4D due to its inexpensive price, user friendly menus, and reputation for being good at modeling images taken using convergent photogrammetry as opposed to parallel photogrammetry.

To speed up the processing time, models were built and stored on the Sirius server at CAST. This provided more physical memory (25 Gigs of Ram) as well as enabling processes to be controlled and monitored remotely from the author's iPhone. Even with the extra memory, it was necessary to create cave models in "chunks" which were later aligned and merged together to form complete cave models. Model construction followed the standard PhotoScan workflow: add photos, align photos, build dense cloud, build mesh, build texture (Agisoft, 2016). After settings were chosen, the pipeline was typically executed in the proper order automatically using the batch process tool. There was some light experimentation with using python code to automate batch processing and store a record of provenance and all settings and parameters used. However, this idea was eventually dismissed as being outside the scope of the research.

Before processing, photos were first divided into chunks and imported into PhotoScan. Each chunk was processed independently using the same sequential workflow and then aggregated into one model at the end of the processing.

Photo alignment was set to high accuracy, pair preselection disabled, with a default key point limit of 40,000 and a default tie point limit of 4,000. A mask was not used. It is during this alignment process that the software automatically detects the make and model obtained from the EXIF data and makes the appropriate calibrations based on the collection of images and the specifications of the specific camera used to capture them.

The dense point clouds for most models were created using the "medium" quality setting as dense point clouds created with the quality set to "high" often used up 100% of the available physical memory leading to very long processing times, and in some cases, failure to process. Depth filtering varied between moderate and aggressive to retain the most points while filtering noise out from outlier points and floating model pieces not attached to the main model. Depth maps were not stored for reuse.

For creation of the mesh the surface type was set to arbitrary, which is recommended for closed structures such as buildings or caves (Agisoft, 2016). The mesh models were created using the dense cloud as the source data, using the default medium face count. Interpolation was enabled with point classes set to "all".

Texture was created using the generic mapping mode from all cameras with the blending mode set to Mosaic. Texture size and counts were set to the defaults and color correction was not used.

Individual chunks were aligned using the camera based method, high accuracy setting, and default point limit of 40,000. Images were not preselected. After alignment, both the dense clouds and models were merged together. Occasionally the area where two chunks were fused together was noticeable. One possible method of getting rid of this is to merge just the point

clouds, then build the mesh for the entire merged point cloud. This however, almost always required more physical memory than one was available and resulted in a failure to process.

Lastly, most models required some post processing that could not be automated. The gradual selection tool was first used to get rid most of the extra floating pieces around the model. After this, any extra unwanted pieces of the model were removed using the rectangle selection tool. This tool also served as a quick means of creating temporary cross section views of the model.

4.4 Exporting Models to Useful End Products

Cave models created and viewed in PhotoScan are no doubt useful and informative by themselves. Finished structures can be rotated and viewed from every angle with the ability to zoom in on areas of interest. While it is possible to view the interior of models in PhotoScan, navigating and exploring the inside of the caves proved to be somewhat awkward and frustrating. Additionally, these products are difficult to share with people who do not have PhotoScan. For this reason numerous exportable end products were evaluated.

Accessing the file, "export model" menu in PhotoScan allows the user to export the model in a wide variety of file formats. Models were often first exported to 3D PDF, which allowed for them to be easily shared and viewed by anyone with a recent version of adobe reader. These 3D PDF files typically only take up a 60-160 megabytes. The somewhat compact nature of this data could potentially allow for 3D PDFs to be stored in a cave database alongside more traditional 2D maps, cave entrance photos, and other data.

To view cave structures in ArcScene, they were first exported from PhotoScan as VRML (.wrl) files. These files were then imported to ArcScene using the Import 3D files tool which outputs to a multipatch feature class. Models first appear without any color and must be replaced

using the editor toolbar. After replacement with the same model, the model will show up in color, allowing the original no-color model to be deleted. The camera was the re-centered on the new model using the center on target tool. Using the animation toolbar in conjunction with the fly function, fly virtual fly though videos of the cave were recorded. The animation toolbar was also used to create videos of caves spinning 360 degrees as if they were spinning on a turntable.

The Unity game engine provided the most interactive and immersive environment for viewing the caves. The game engine can be downloaded for free, and finished game applications can be shared easily. Unity allows for the user to utilize the arrow keys on the keyboard to fly through the model at their own pace, stopping and turning around or going down a different passageway as they choose. This proved to be the most useful way to explore models and to examine areas where the mesh was incomplete or of poor quality.

To do this, a .3DS file was exported from PhotoScan and imported as an asset to Unity. Basic flat terrain was created long with a directional light in the sky to provide some exterior light around the cave. A first-person controller was equipped with a flashlight which allowed for a cave exploration simulation to be made where the user could walk around the dark cave in first person with only the small light to see.

In order to share the caves in a more traditional 2D map view, ArcMap was used to create 2D footprint maps. Using PhotoScan, the orthomosaics were first built, georeferenced if survey data was available, and then exported to .tif format. A model was designed in ESRI's model builder which automatically takes the orthomosaic, reclassifies all non-zero pixel values to "1", converts from raster to vector, uses a positive buffer to buffer out any internal holes, and finishes with an equal and opposite negative buffer to return the outside boundary of the cave to its original extent. The result of this is a 2D footprint map of the cave's extent in the X-Y plane.

Cross sections were then made from the 3D model and added to various locations on the footprint map. If the orthomosaic was georeferenced before it was exported, a north arrow and scale was added.

Along with these final products, final reports were generated within PhotoScan which include detailed information on calibration coefficients, camera residuals, RMSE of the point clouds, as well as a breakdown of errors in the control network.

4.5 Control Target Survey and Georeferencing Models

Photogrammetric models initially only possess a very rough scale based on the focal length of the camera. To get meaningful and accurate information such as measurements of passage dimensions, areas, volumes, locations, and orientations, models must be georeferenced. To do this, X,Y,Z coordinates must be entered at various unique points in the model. While early attempts used distinct natural cave features, or objects like water bottles for targets, it was found that the printable coded targets found within the Agisoft software worked best. The targets are easy to spot and are all slightly different so that each target represents a different unique marker number in the software. The coding of the targets allowed the software to scan and detect all the targets without the user having to manually find and click the center of each one. Ideally, control targets should be placed evenly across the surface of the photogrammetric survey area, and then simply surveyed with GPS equipment. Clusters, or linear placement of control points is not recommended. However, in this case, the highly linear nature of caves and tunnels made this distribution of targets unavoidable. An additional challenge was surveying control targets while inside caves where there is no GPS satellite reception. Several methods were developed for georeferencing underground models despite the lack of GPS availability.

The first method was a quick and dirty one where 3 targets where placed around the entrance of the cave and surveyed to give a rough idea of location and distances in the model.

The second method used a traverse to create a traditional cave survey line from one external GPS coordinate at the cave entrance, to multiple internal survey stations throughout the cave. All External GPS coordinates were obtained using a highly accurate Leica GS15 with a CS15 Controller and a GS15 Pillar Tripod. The rapid static method was used throughout the research to obtain data in the Arkansas State Plane North coordinate system. It should be noted however, that the accuracy of the initial GPS point only effects absolute accuracy and the quality of coordinate locations, while lengths, widths, heights, and volumes of cave passages rely entirely on the accuracy of the traverse data. Cave dimensions and volumes can be obtained with only data from a traverse, simply setting the GPS point to some coordinates in the general vicinity of the cave, or even (0,0,0). A change in the initial coordinate will shift all other control points in the same direction by the same amount.

To calculate the (X,Y,Z) coordinates of all survey stations along the survey line, distances, azimuth, and clinometer data were used with the following equations inside of a Microsoft Excel document. These equations are similar to the standard equations used to convert spherical coordinates to Cartesian coordinates but are adapted to work with a degrees from the horizontal component instead of a degrees from the vertical component. The equations were derived by the author and tested with trial and error for validity. Because the sine of an angle is equal to the cosine of its compliment, the resulting set of derived equations represents the exact same set of standard equations used to transform from spherical to Cartesian coordinates except that all trigonometric functions have been replaced with their cofunction.

$$\Delta X = [R*\cos(\zeta)]*\cos(\alpha) \quad (1)$$

$$\Delta Y = [R*\cos(\zeta)]*\sin(\alpha) \quad (2)$$

$$\Delta Z = R*\sin(\zeta) \quad (3)$$

In these equations, the delta values represent the change in X, Y, and Z coordinates from the first station to the second survey station, which are calculated from the azimuth value in radians, α, the zenith value in radians, ζ, and the true distance between the stations in meters, R.

Cave survey data is typically taken in azimuth degrees, vertical degrees from horizontal, and feet between stations. All coordinates were taken in the state plane Arkansas North (meters) coordinate system, so all distances measured in feet were first converted to meters. Excel works in radians mode only, so all azimuth degrees and degrees from horizontal were first converted to their equivalents in radians before they could be used in the above equations.

4.6 Accuracy Assessment

Once models were created and georeferenced, some measure of quality and correctness needed to take place. To start with, footprint maps from the 3D models were overlaid and visually compared to any existing cave survey maps. This process was done in Microsoft Word, where the white paper background of the cave sketch could be made transparent leaving only the sketch of the cave. The both graphics were manually sized and positioned for the best possible fit and examined for similarity. This allowed for a basic visual assessment but no quantitative assessment in accuracy. Additionally, even if one quantified the exact deviation between the photogrammetrically derived map, and the hand drawn map, one could not actually say that one is more correct than the other anyway. The best control to compare to would be a LIDAR scan, but this equipment was not available for the project.

A more quantitative approach was taken in Davis Creek cave, where left and right dimensions at survey stations where measured inside the georeferenced model and compared to LRUD data acquired in the cave. While this cave was meant to be the "flagship" cave of the project in terms of assessing the quality of georeferenced cave models, the large passage widths ended up pushing the limits of the system resulting in many holes in the side walls and ceiling. Regardless, the comparison in passage width measurements derived from the virtual model and widths measurements measured in real life were compared simply noting where the distance left or right of the station could not be properly measured due to a hole in the model on the side wall at that particular location.

As previously mentioned, it is difficult to assess whether an abstract structure like a cave is really modeled correctly because there is no perfect representation with which to compare it. Nearing the end of the research, a manmade tunnel was also modeled. Whereas it was nearly impossible for the eye to detect distortions in the cave images, bent and warped vertical support beams were quickly recognized in the tunnel images allowing for a test to be done to see how the PhotoScan software would handle these distortions. The trend of the tunnel was straight compared to the natural unpredictable cave passages, which meant that any deviation from this straight line would represent error in the model. While the trend was in the X-Y plane was very consistent and predictable, some slight complexity was added by the floor which slopes gently towards a central drain followed by an upward slope.

5. Results/Discussion

5.1 Aspen Cave

The pilot study and proof of concept occurred in Aspen Cave. The first attempt used a helmet mounted Go Pro and Princeton Apex headlamp. These images were processed online using Autodesk 360 Recap and resulted in only a model of the outside of the cave. It was quickly realized from this experiment that more light was needed. A survey "rig" was created consisting of a GoPro attached to a bright portable floodlight with an iPhone attached. Returning later with the new method, the first model of the inside of the cave was generated. It was noted that the 2 second time lapse mode was effective for acquiring pictures outside of the cave, but that this resulted in blurry photos in the darker more confined environment of the cave. For this reason, still photos were primarily used to model the interior of the cave which were more time consuming to acquire, but were better focused. 360 Recap offered very little control over how the model was being processed, so these images were then processed in Agisoft PhotoScan. This allowed for more hands-on model construction, as well as the ability to experiment with creating the model in "chunks" which were later aligned and merged together. The cave was processed in 4 chunks each containing around 20 images. Aligning each chunk with the other chunks by camera location initially failed. To remedy this, some overlap was needed between the image subsets. For each subsequent chunk, the last three photos from the previous chunk were added. This allowed the four chunks to be merged into one complete cave model which consisted of 19,944 tie points, a dense cloud of 15,469,416 points, and a textured 3D model with 1,028,256 faces. As reported by the PhotoScan processing report, the point cloud had an RMSE re-projection error of 1.12 pixels and a maximum re-projection error of 3.633 pixels. The quality of the mesh turned out well with only a few small holes zooming through the cave model in the forward direction. (The direction that the camera was pointed.) Looking at the model in the

reverse direction, there were many small holes and black areas representing no data. These represent shadow areas that the camera could not see while moving through the cave in the forward direction. Small dark rings were also visible where the chunks were welded together. To make the model universally shareable, it was exported to 3D pdf format. This exported file took up 59.7 MB of storage space and allowed for anyone with adobe reader to interactively view a slightly lower resolution version of the model.

Fig 3. Aspen Cave viewed as 3D PDF

While rotating the cave and viewing its exterior was simple, scrolling through the cave to the very back was difficult, and as one zoomed to the very back, the model began to disappear. Because of this, an attempt was made to also create an accompanying traditional 2D cave map based on an orthomosaic constructed from the X-Y extent of the 3D model. The intent here was to both present an easy to understand plan view of the cave, as well as various 3D cross section views of the model. While cross sections can be made anywhere in PhotoScan, this first

experiment used the individual chunks leftover from creation of the model as rough cross sectional views.

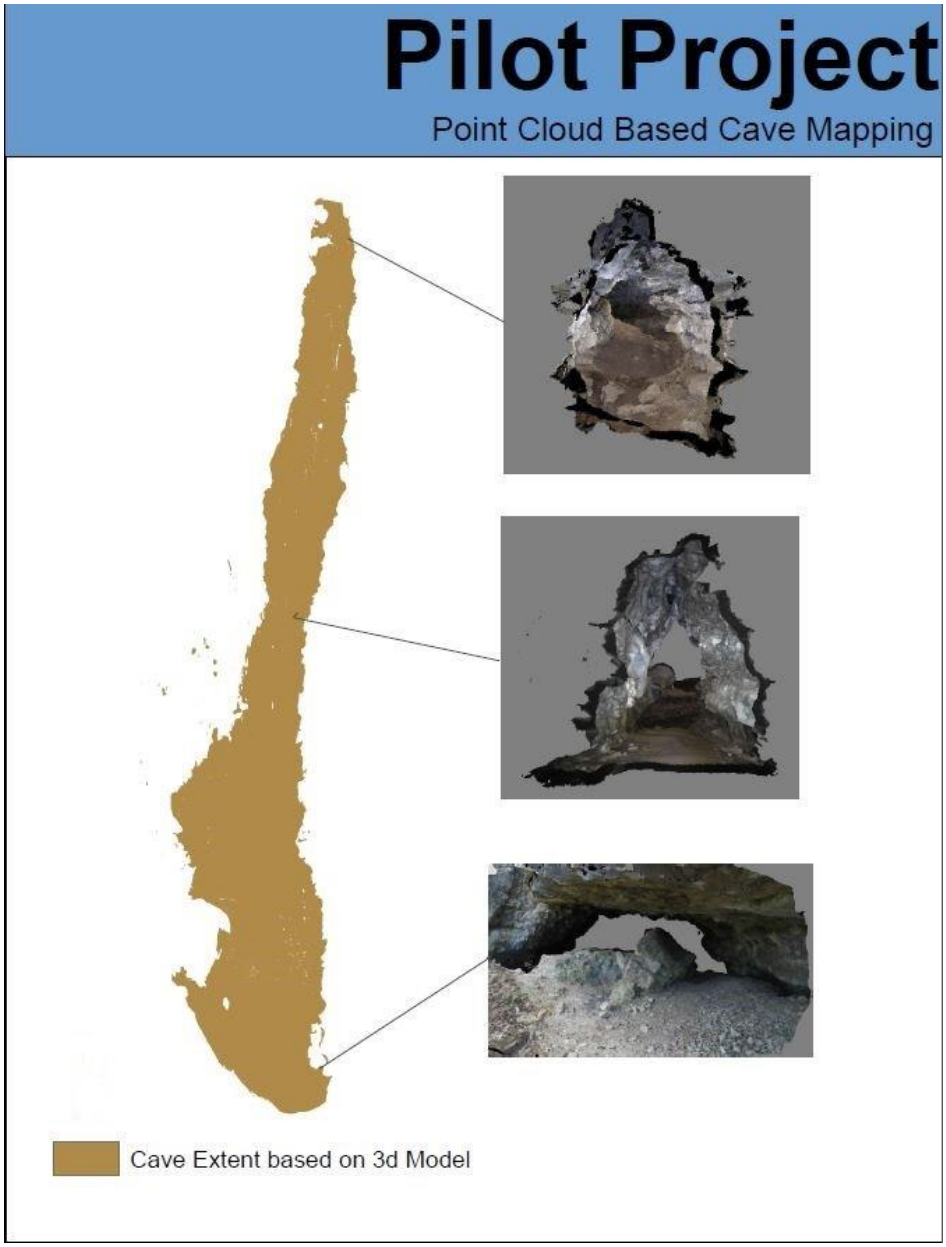

Fig 4. 2D map created from orthomosaic based on X-Y extent of the 3D model

5.2 Birch Cave

Birch Cave offered an opportunity to study the limits of the methodology in a much larger cave. Still images were taken around the entrance of the cave, and down the first 150-160 meters of passage to a large column. These images were divided into 7 chunks containing 75 to 144 images per chunk. Each chunk contained around 10 images in common with the previous chunk to ensure they could be aligned and merged properly. In total, the model took just under 19 hours to process. The finished product consisted of 151,239 tie points, a point cloud of 66,782,453 points, and a model with 4,435,017 faces. According to the PhotoScan processing report the point cloud had a RMS re-projection error of 2.57 pixels with a maximum re-projection error of 84.078 pixels. The resolution of the model was listed as 1.64mm/pixel. While the completed model does represent the general trend of the cave passage, there were numerous large holes in the side walls and ceilings. Passages exceeding 9-11meters (30-35ft) in width, especially large rooms over 30 meters (100ft) wide resulted in missing left and right walls. An attempt was made to capture the large room just after the entrance by moving around the perimeter of the chamber while pointing the camera towards the center, but there was not enough light to light up the far walls. Instead a linear path was made through the large room, attempting to capture as much information on this path as possible as it lead up to a more confined linear passage. Sections of this more confined linear passage turned out much better than the large room, but had challenges of their own. While average ceiling height remained consistent, there were several areas of the ceiling which shot up dramatically. These vertical features ascending from the main walking passage were difficult to capture. Even with effort taken to maintain overlap, for the most part, any picture taken with the camera pointed upwards was not aligned with the rest of the images facing down passage resulting in many holes where

the vertical extent of the ceiling could not be imaged. At the end of this passage, a large column was modeled which turned out complete but was not very high resolution. Because of this, a separate individual model was created of this feature to capture it in the greatest detail possible. To share the results of the 3D model universally with others a 3D rotating model and virtual fly through of the cave was created in ArcScene. However, color could not be added to this model, possibly do to the large amount of faces in the mesh.

A challenge of this project is to present results which are inherently 3D in the 2D format of this research paper. Due to the large size of the cave model and the differing characteristics of each of the 7 chunks used to reconstruct the cave, they will each be discussed separately.

5.2.1 Chunk 1

Chunk 1 modeled an approximately 20 meter by 20 meter area outside of the cave. This took 144 photos and created a point cloud with over 7 million points. Despite numerous shadows in the images, the quality of this first exterior model was very good. The creek bed, trees, survey equipment, and six control targets are clearly visible along with the words “keep out” on the rock face near the entrance. The purpose of this large entrance area chunk along with the 6 targets was to allow for georeferencing of the entrance area if georeferencing the rest of the cave was not possible. In the end only one of these control points was used.

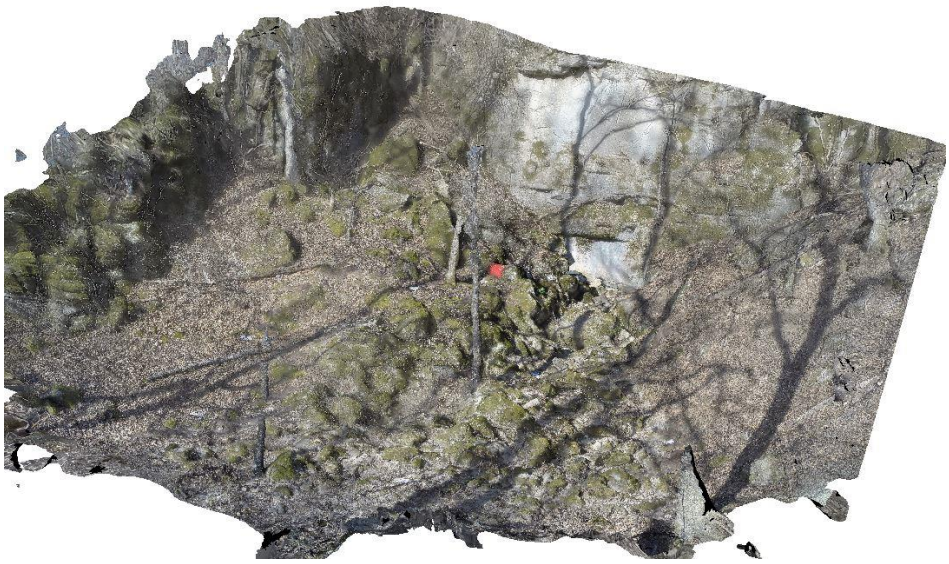

Fig 5. Exterior of cave

This first part of the model captures the tight crawlway entrance into the cave and successfully aligned and merged this thin narrow piece of mesh between the large exterior model and large interior model much easier than expected.

Fig 6. Screen capture of the cave entrance with mossy rocks scattered along the creek bed and “keep out” faintly visible on the rock face.

Fig 7. Close up showing detailed model of tight crawlway into the cave.

Fig 8. Screen capture showing thin connection between exterior and interior portions of the cave model.

5.2.2 Chunk 2

The second chunk modeled the tight entrance as it gradually descends and opens up into a large room. 141 images were used to model this section of the cave which produced a point cloud of about 15.7 million points. A large stalagmite at the end of the chunk was used as the second control point. While the ceiling and floor turned out well, a significant majority of the left and right side wall were missing. In this first large room, it was difficult to capture the entire room in the field of view of the camera. It was also challenging to light up the other side of the room at such a great distance.

Fig 9. (Left) Illustrating missing left and right walls as the cave opened up into the expansive room. (Right) Plan view of Chunk 2 with cave entrance at bottom of screen capture.

5.2.3 Chunk 3

Chunk 3 represents the central part of this large chamber. This chunk is an even more extreme example showing the floor and ceiling along the linear path of the camera, but leaving out the nearly all of the sidewalls of the cave. This section of the cave was created from 107

images which created a point cloud of roughly 11.7 million Points. This section captured a rill developing across the floor of the cave from water draining towards the entrance.

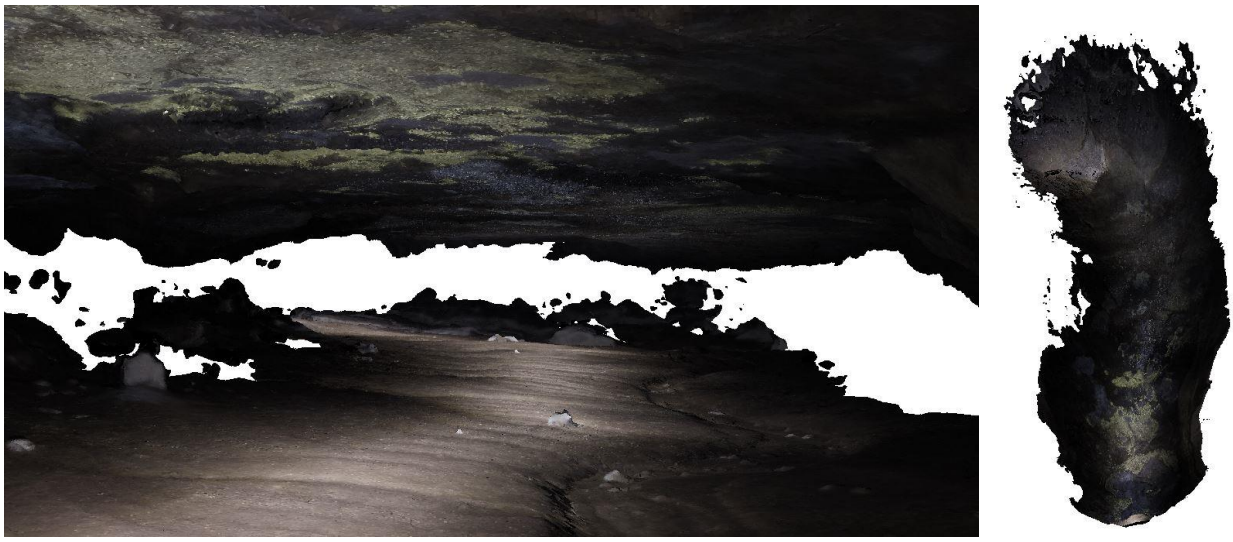

Fig 10. (Left) Illustrating missing left and right walls in the middle of the large room. (Right) Plan view of Chunk 3 with the top portion representing further in cave and bottom portion closer to the cave entrance.

5.2.4 Chunk 4

The fourth section of the model represents the end of the large room as the cave walls begin to taper off into a more confined linear passage of about 10-11 meters (35 feet) of width. This section used data from 76 images and created a point cloud of 7.6 million points. This chunk is much more complete in nature than previous sections modelling the ceiling, left wall, and boulder covered floor. It is however missing a significant part of the right wall which extends a good distance from the path of the camera.

Fig 11. Shows marked improvement in the completeness of chunk 4 as the cave tapers off towards a linear passage. (Right) Plan view of chunk 4 with top part representing the beginning of linear passage.

5.2.5 Chunk 5

Chunk 5 marks a shift from the large beginning chamber unto the first of three sections of linear passage. This confined passage way had much better results with complete left and right walls. There were however, several holes in the ceiling due to abrupt changes in ceiling height. The chunk took only 62 images which generated a point cloud of 6.9 million points.

Fig 12. (Left) This chunk of linear passage was very successful, besides the holes visible in the plan view of the model. (Right) Plan view of chunk 5.

5.2.6 Chunk 6

Chunk 6 was the second section of linear passage. This section used 73 images and produced 9.2 million points. This chunk was similar in nature to the previous chunk, widely successful with the creation of the floor and sidewalls, but struggled to model the ceiling in areas with sudden and dramatic increases in height. This section of the passage begins to be more airfoil shaped, tapering off quickly to a low ceiling along the left wall of the cave.

Fig 13. (Left) Screen capture looking down passage through chunk 6. (Right) Plan view of chunk 6.

5.2.7 Chunk 7

Chunk 7 was the final chunk of the cave model representing just the first 150-160 meters of Birch Cave. This final section modeled a beautiful cave column at the end of the chunk. While the right-hand wall turned out very well, almost all of the left-hand wall was missing as well as the central part of the chunk. It is unclear why this occurred, however the airfoil shape seen in the last chunk tapers off even sharper along the left wall here, along with an increased width

from about 10.7 meters to 12.2 meters (35ft to around 40ft). The wider passage along with the more sharply sloping ceiling along the left wall most likely cast a dark shadow along that portion of the cave wall.

Fig 14. (Left) Screen capture looking down passage through chunk 6 towards large column. (Right) Plan view of chunk 7.

Fig 15. High resolution model of cave column processed independently in its own chunk.

5.2.8 Georeferencing the model

For the model to have proper orientation and scale it had to be georeferenced. Additionally, spatial reference was important in defining up and down directions in the model so that it could be rotated naturally in ArcScene. (Initially tilt and roll functions worked but the yaw function, that is, rotating the model as if on a turntable was not functional. Georeferencing the cave model was challenging as clearly there was no GPS reception underground, and a cluster of control points at the entrance would likely do very little to provide accurate spatial information far down the length of the passage. Because of this, a method was developed which used a single GPS point at the entrance and a basic survey line traverse throughout the length of the cave. While there were 11 survey stations along the traverse, only 6 of these stations were

selected to be control points, due to their unique, easily recognizable locations. An Excel spreadsheet was used to calculate the approximate GPS coordinates of each control point along the survey line. Figure 16 shows the overall distribution of control points throughout the cave.

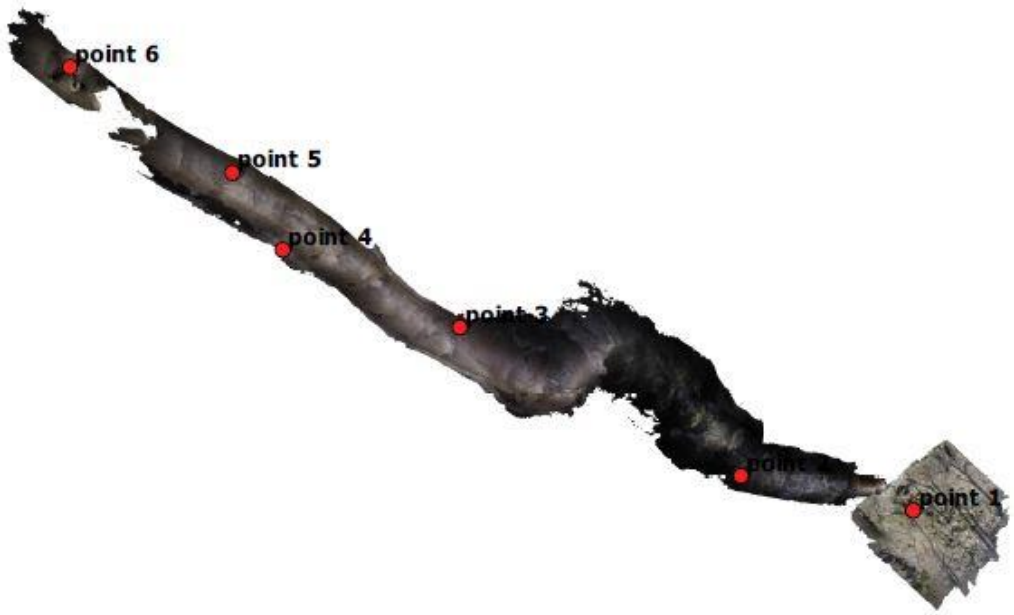

Fig 16. Control Points

The initial GPS control point at the entrance was taken by a Leica GS15 using the Rapid Static method. The GPS unit occupied the location for 1 hour and 14 minutes. Unfortunately, correction via the National Geodetic Survey's OPUS (Online Positioning User Service) website failed to correct the resulting RINEX file retrieved from the GPS unit. This may have been due to the thick tree cover and proximity to the steep hill side in which the cave is located. Nevertheless, even without post processing, the occupation of more than an hour likely resulted in a point more than accurate enough for the application. In fact, while the GPS point does affect the absolute accuracy of locations in the cave, it has no effect on relative accuracy between control points, which is wholly reliant upon the traverse. Unfortunately, the calculated

coordinates of each control point could not be listed in order to protect the cave and respect the owner's wishes. Instead however, an analysis of control point coordinate quality is presented in table 3.

Table 3 Control Point Quality

(Values from PhotoScan Processing Report)

GCP	X error (m)	Y error (m)	Z error (m)	Total (m)
Point 1	1.47091	-0.125357	-0.292624	1.50496
Point 2	-0.807128	-0.212727	0.930479	1.25
Point 3	-1.26324	0.792292	-0.712222	1.6525
Point 4	-0.479499	0.233919	-0.182537	0.563878
Point 5	-0.0529091	-0.679768	-0.246493	0.261111
Point 6	1.12738	-0.618425	0.5032222	1.38082
Total	**0.99285**	**0.434066**	**0.548633**	**1.21456**

The traverse data was produced by Kayla and Pradeep Sapkota using a Sunnto clinometer/Compass and a Disto laser range finder. All traverse survey data used to calculate in-cave GPS coordinates is listed in Table 4. Station D0 represents a vertical offset from the recorded initial ground GPS point, .9 meters up the central vertical pole of the tripod. Horizontal and vertical angles were checked with back shots, and redone until they agreed within two degrees. Distances between stations were precisely measured while LRUDS were estimations, typically to nearest .15 meters (.5ft). All distances were surveyed in feet, but converted to metric here to maintain consistency with the rest of this paper. Dashes in the LRUD section of the table represent stations which were outside of the cave where distance to ceiling and other measurements were not applicable. Down measurements with an additional number in parenthesis represent a station located on an object or ledge with the measurement all the way to the true floor of the cave represented in parenthesis.

Table 4. Survey Traverse Data (Survey by Kayla and Pradeep Sapkota)							
Station/GCP	Distance (m)	Bear. Angle (Front/Back)	Vert. Angle (Front/Back)	Left (m)	Right (m)	Up (m)	Down (m)
D0 / GCP1				--	--	--	.90
	5.34	339.5 /159.0	-10.5/9.5				
D1				--	0.15	--	0.24
	2.12	236.0/55.0	-4.5/5.0				
D2				.61	0.15	.91	0
	2.14	248.5/68.0	-10.5/10				
D3				1.83	2.44	.24	0 (+0.15)
	21.82	278.0/99.0	-3.0/4.0				
D4 / GCP2				8.23	9.45	1.62	.30
	33.59	327.5/148.0	2.5/-2				
D5				27.13	8.23	2.29	0 (+.46)
	18.38	238.5/59.0	2.0/-3.0				
D6				10.06	20.42	2.74	.76
	14.66	292.0/113.0	-0.5/-2.0				
D7 / GCP3				4.57	6.10	1.98	.91
	33.53	294.0/114.0	-1.0/0.0				
D8 / GCP4				1.52	9.45	.30	.61
	16.11	326.0/147.0	0.0/0.0				
D9 / GCP5				8.23	2.74	3.96	.61
	16.28	280.0/100.0	3.0/-4.0				
D10				2.44	7.92	.46	1.52
	20.18	321.0/142.5	0.0/0.5				
D11 / GCP6				9.14	2.92	1.92	1.52

5.2.9 Accuracy Assessment

Birch Cave was originally intended to be the "flagship" cave of the research project. It was hoped that a large 1.5km long model could be constructed, accurately georeferenced, and then tested for accuracy. Unfortunately, the large size of the cave really pushed the limits of the method. Even in just the 150-160 meter section that was modeled, a large portion of the cave

walls were missing. Because of this, more time was not invested in advancing the model further into the cave, or improving the survey data used to georeferenced it. Because of the many missing sidewalls, Birch cave does not represent the optimal situation for comparing real world measurements to model measurements. None the less, a comparison of left and right measurements at each station was made between the survey data, and what was measured in the virtual model. This comparison is listed in Table 5. Here, values in red with an asterisk indicate that there was a hole in the model at this location which prevented the full extent from survey station to wall from being measured.

Table 5. Left-Right Measurements Comparison

Station/GCP	Virtual Model in PhotoScan		Real World Survey Data		Error (m)	
	Left (m)	Right (m)	Left (m)	Right (m)	Left	Right
D0 / GCP1	--	--	--	--	--	--
D4 / GCP2	*2.56m	9.48m	8.23m	9.45m	--	.03m
D7 / GCP3	6.55m	*2.32m	4.57m	6.10m	1.98m	--
D8 / GCP4	1.16m	9.42m	1.52m	9.45m	.36m	.03m
D9 / GCP5	8.26m	3.66m	8.23m	2.74m	.03m	.92m
D11 / GCP6	*4.97m	2.65m	9.14m	2.92m	--	.27m

If the areas where the wall was entirely missing is ignored, 3 out of the 7 left-right measurements in the virtual model agree almost exactly with the real-world measurements. The worst discrepancy occurred at station D7 where the left measurement in the virtual model was 1.98 meters in excess compared to the real-world measurement. Referencing table 3, this station had the worst total error at 1.65 meters. There are several considerations when attempting to identify the sources of these errors. First, there was limited precision in selecting target locations with the mouse. While care was taken to select the exact portion of the stalagmite, rock, or other object that was used as a survey station, there was certainly some small error in selecting the

exact location of the survey station on the natural object. Similarly, there was a small degree of error derived from using the measuring tool within PhotoScan. Care was taken to place the model in the "top" predefined view looking straight down on the X-Y axis. Even despite this, the precision of the measuring tool was limited and each time the measurement was taken resulted in a very close, though slightly different value. Front shots were allowed up to two degrees difference with back shots. Even an error of two degrees could make a significant impact on the quality of subsequent control point locations further down the traverse line. Lastly, it should be noted that often LRUDs are somewhat subjective. The exact angle that a surveyor points the Disto from the station to the wall may influence the range to the wall slightly. This is exacerbated further where there are bulges or objects along the wall where left measurements may vary by a third of a meter or more simply by shooting to one place on the wall versus another. LRUDs in this cave survey were typically only recorded to the nearest half foot, meaning that differences of .03m (0.1 ft) in the table are not significant.

5.3 Cedar Cave

At around 77 meters (253ft) of survey length, Cedar Cave was much bigger than the pilot project in Aspen Cave but also a great deal smaller than the large section modeled in Birch Cave. It took a total of 296 unique images to model the cave. Some of these images were rear facing photos (towards the entrance of the cave), which was an experiment to see if both front facing and rear facing images could be aligned in the same passage way to eliminate data holes when viewing the cave passage in the opposite direction that the camera traveled through the cave. Images were first taken from the entrance area towards a two-way split, then down the left side arm of the cave in the forward direction, then in the reverse direction back towards the junction, finishing with modeling the right arm of the cave in the forward direction.

Initially, there was an attempt to process all 296 images together to build the model all in one chunk. This resulted in a model of the central part of the cave with the end of both arms of the cave as well as the entrance area missing. This model of the central portion of the cave consisted of 142,692 tie points, a dense cloud of 23,414,135 points, and a mesh model with 1,291,670 faces. To remedy the missing pieces three more chunks were created utilizing: 28 images for the left arm, 31 images for the entrance area, and 70 images for the right arm of the cave. All 4 chunks were easily aligned and merged. Unfortunately, the mesh of the entrance chunk was closed at the far end where it entered into the main passage. After these sections were aligned and merged, this mesh divider between the two adjoining sections of cave passage was manually selected and deleted. The final model was somewhat larger consisting of 219,881 tie points, 38,476,633 points in the dense cloud, and a mesh model made up of 2,107,132 faces. The point cloud had an RMS re-projection error of 1.23 pixels with a max re-projection error of 56.58 pixels.

There were very few holes in the model, the most of significant of which were located holes in the ceiling at locations where the passage bulged out and the ceiling height increased. Viewing the left arm of the cave in reverse (toward the cave entrance) versus the right arm of the cave, there were far less black “data shadows” along the cave walls. This lends support to the method of taking pictures both down cave passages and back in the reverse direction. While this lead to less black spots when viewed from the other direction, it did not improve the geometry of the mesh, and added some extra processing time.

Fig 17. Hole in the top of small room with elevated ceiling height.

The passages in this cave were about 1.5m by 1.5m (5ft by 5ft) representing the tightest cave passage studied in the project. Crawling through the cave taking pictures lead to an interesting observation. In aerial photogrammetry, flying height is an important factor, determining both the ground resolution, as well as the geographic extent of the ground being captured in each image. Flying closer to the ground, if flying slow enough, can improve spatial resolution, but will require taking pictures more frequently per distance traveled, as well as requiring more transacts back and forth across the target area. On the contrary, during high altitude image capture, it takes far less photos to capture a large area, though the cost is often a much coarser spatial resolution. In the case of cave passage photogrammetry, flying height can be replaced with passage diameter. In the larger open walking passages of Birch Cave, one could walk for a few steps before snapping another image, while in Cedar cave, crawling a third

of a meter forward immediately required another image to maintain overlap and capture changes in the scene as they occurred.

Fig 18. Crawling passage approaching two-way fork.

Cedar Cave was georeferenced to the Arkansas State plane coordinate system using 3 GPS coordinates around the entrance area. 3D control targets consisted of Nalgene water bottles, which were surveyed with a Leica GS15 unit in in rapid static configuration. This gave the cave a rough reference of up, down, north, and the ability to very roughly estimate widths and lengths inside the cave model. The control network, as listed on the PhotoScan processing report, had an error of about 1.6 meters in the X and Y directions, and a total error of 2.4 meters.

An existing survey sketch of the cave allowed for a relative test of accuracy to occur. This compass and tape survey was overlaid over the top of the X-Y extent of the

photogrammetric model in Microsoft word. This allowed for the white paper background of the survey sketch to be made transparent leaving only the sketch of the cave passage walls and other accompanying information. The two images were scaled and oriented manually for best fit, revealing a close match, besides some small deviations in the tips of each arm of the passage. Note that a second connection between the two arms of the passage is observable in the sketch but not the model. This connection was noted in-cave, but was too small to crawl through and scan with the camera.

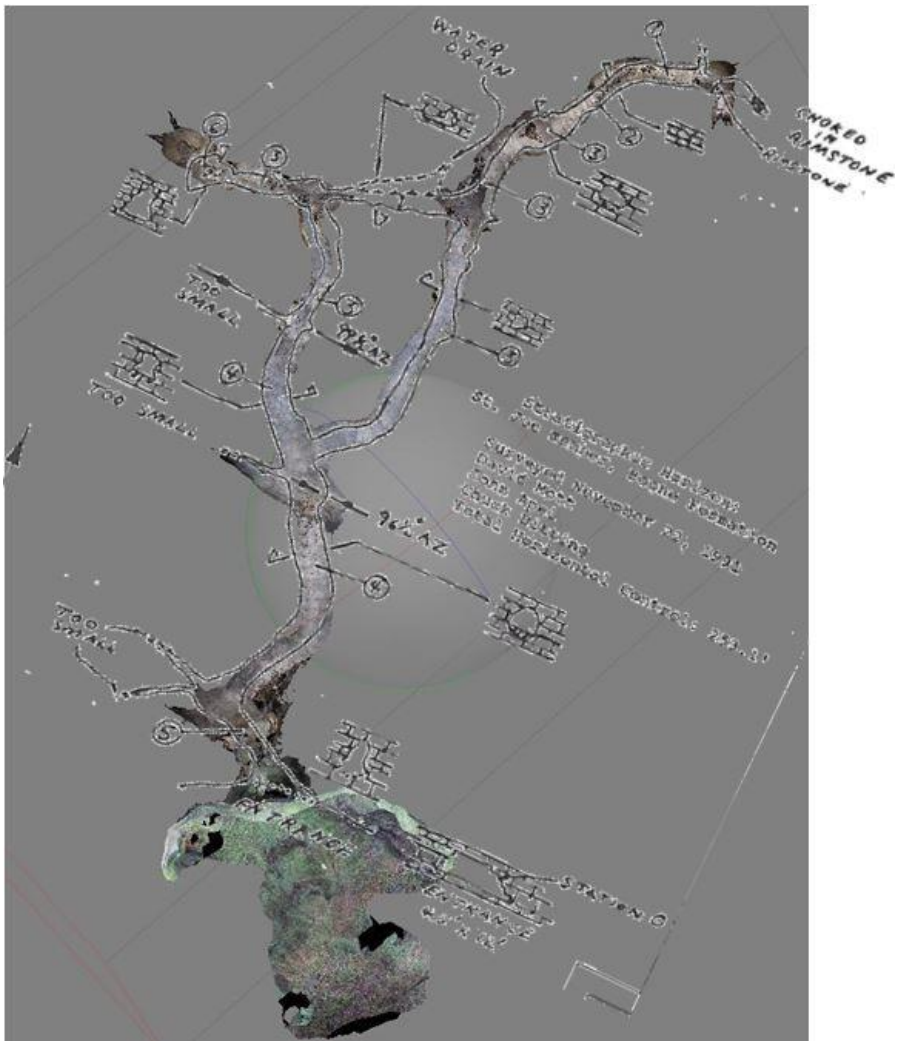

Fig 19. Traditional compass and tape survey overlaid over plan view of 3D photogrammetric model.

5.4 Dogwood Cave

Dogwood cave consists of about 60m (200ft) of sinuous walking passage with a small stream running along the floor. The entire cave was modeled with 130 images. An additional 88 rear facing images were taken from the back of the cave returning to the entrance, but these images were never successfully aligned with the rest of the photoset. The model was first run all as one chunk with the set of 218 total images. However, the resulting model only included the back half of the cave. Trouble-shooting began with running the first 41 photos in the photoset to model the entrance area and the passage just after it, which rendered successfully. After this, a quick glance of the groups of photos that did not align revealed a problematic area in the model. This problem area was isolated and constructed as its own chunk of just 12 photos. Once this was complete, the front and rear of the cave were aligned with the middle problematic section, which was missing a large portion of its floor, but was otherwise intact.

The entire finished model consisted of 219,881 tie points, a dense cloud of 38,476,633 points, and a mesh model of 2,107,132 faces. The point cloud had an RMS re-projection error of 1.28 pixels, with a max re-projection error of 39.54 pixels.

One of the challenges of creating this model was locating and modeling the trouble area, a gap between the front and rear chunks were there was not as much data. This weak area can be seen more easily in Figure 20, where an orthomosaic of the model was created and reclassified to show only pixels with a non-zero value. This weak area could have been caused by several things. It should be noted that the passage bends sharply here, and is the first place that the camera directly crosses over the stream. An analysis of image spacing reveals that poor image overlap is also likely at fault. The lack of image overlap is illustrated in Figure 21.

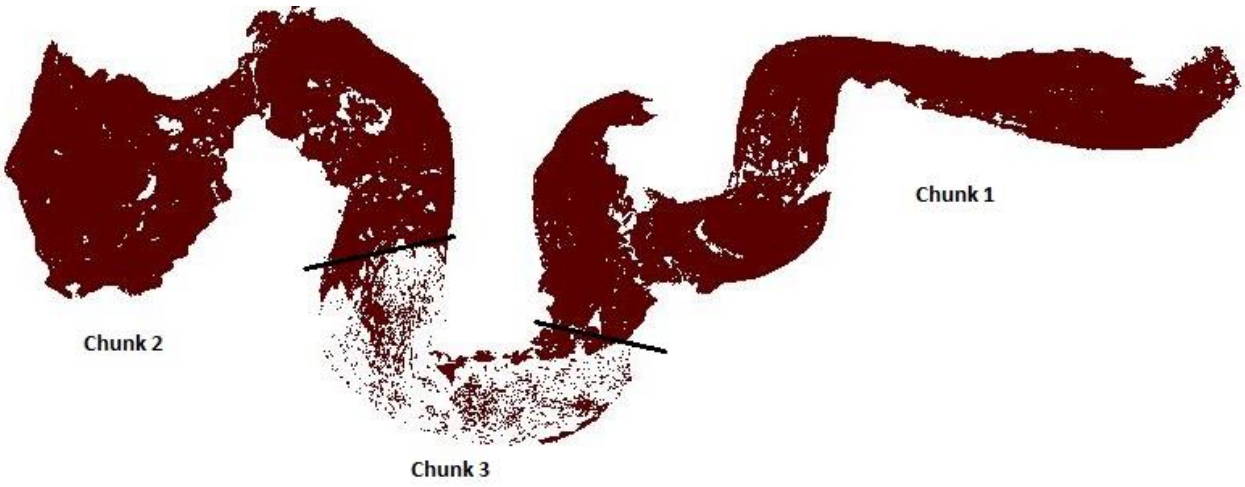

Fig 20. Reclassified Orthomosaic showing weak area with little data.

Fig 21. Screen capture where the ceiling of the cave has been removed to show poor image overlap through the bend. Images 5507-5510 were highlighted in red to show some of the worst image overlap through the abrupt turn in the passage. Note that image 5509 was removed because it was poorly focused creating a gap in the photos just before the bend.

Other issues with this model include a small section of missing walls and ceiling as the entrance of the cave widens into the main passage, as well as difficulty modeling the floor in areas where there was a lot of standing water. The largest hole occurred at the back of the cave where there was a wide pool. These challenging watery areas are illustrated in Figure 22.

Despite these challenges, the rest of the model turned out well capturing both the sinuous nature of the cave as well as the scalloped nature of the walls, which was not readily apparent in person when the images were acquired.

Fig 22. Screen capture of model with ceiling removed to show holes in the floor in areas where there was standing water.

Several end products were created so that the model would be more easily sharable with others. A 3D PDF was created, along with a video of a virtual fly through of the model in ArcScene, and a video of the model spinning as if on a turntable, also generated in ArcScene. This was the first time a color model was successfully rendered in the software by replacing the 3D model with itself using the editor toolbar. The ArcScene fly through of the cave model allowed for the viewing of all parts of the interior of the cave, including those that were difficult to view in PhotoScan. However, navigating the interior of the model with this tool was limited, with only control over the speed of movement and the ability to adjust course slightly up, down,

left, or right while flying through the cave in one direction. The model was then imported into Unity game engine. This software offered by far the best way to interactively fly through each part of the model allowing the user to look or move around in any direction desired. Figure 23 illustrates the mesh model of the cave as viewed in Unity.

Fig 23. Unity game engine allowed for easy inspection of all parts of the mesh, allowing the user to easily move forwards, backwards, left, right, up, or down, inside the model while simultaneously changing the look direction of the camera.

While the main practical use of Unity was the ability to go to and view any part of the interior of the model with ease, a video game style caving simulation was also created which allows the user to control a 3D character and walk around the cave. A spotlight was added projecting from the front of the character to simulate the effect of a flashlight or headlamp in the dark cave. A screen capture from this caving simulation is shown in Figure 24.

Fig 24. Cave exploration simulation created in Unity.

Throughout the project there was an effort to generate not only a 3D model, but also, simultaneously, a 2D map somewhat similar to what would be produced using traditional cave survey methods. This method was improved further in the processing of Dogwood cave, where a model-workflow was designed to automatically take an orthomsaic of the model and output a map of the caves X-Y footprint. The first experiments with Aspen Cave simply took the orthomosaic and reclassified pixel values to "1" or no data. This worked okay, but left holes in the map where the mesh was not complete. This workflow took the process further by converting the reclassified raster to vector format, buffering outward to remove any internal holes, then utilizing an equal and opposite negative buffer to return the exterior cave walls to their original extent. This workflow, and resulting outputs are illustrated in Figure 25.

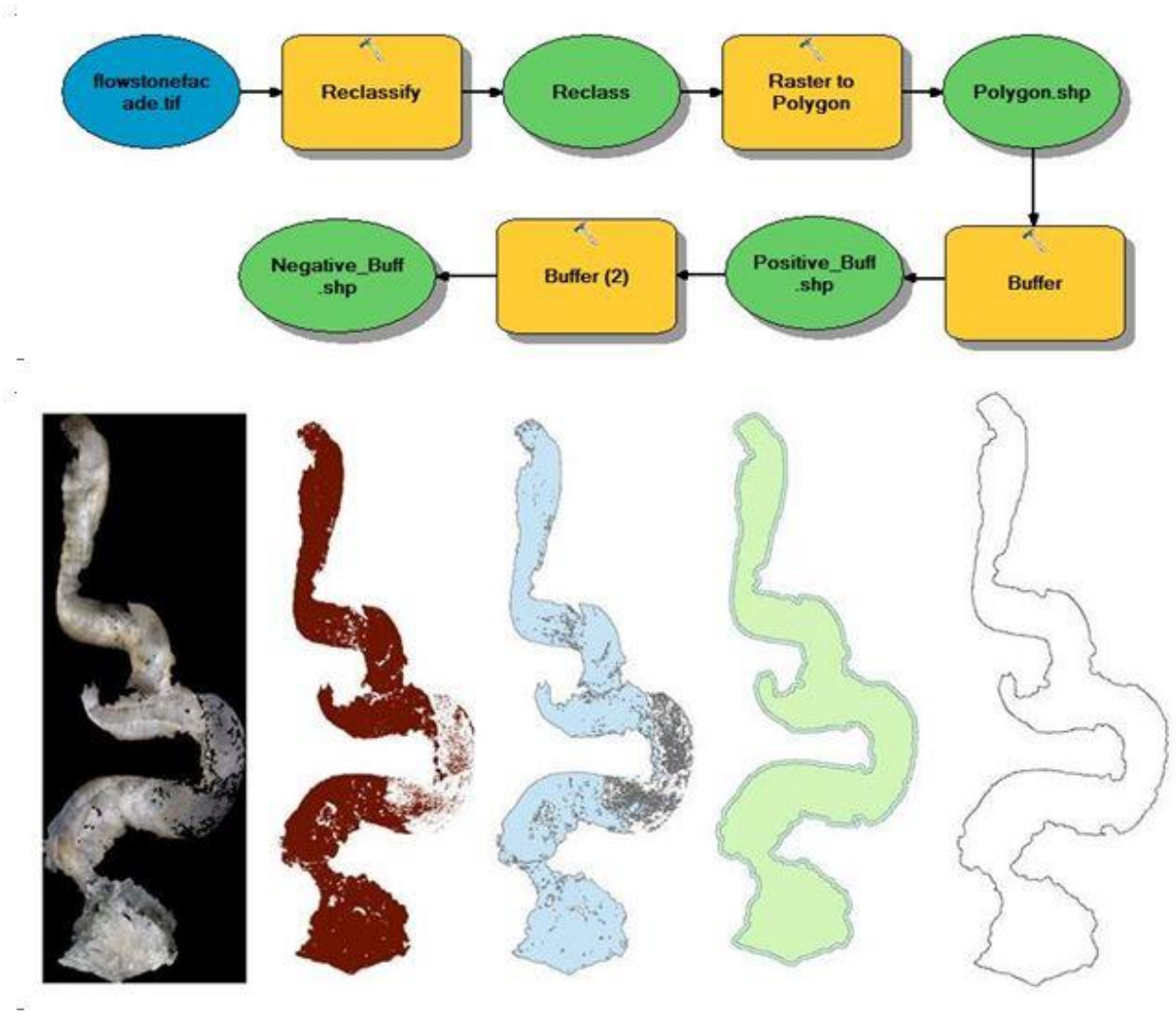

Fig 25. Workflow designed using Esri's model builder which automatically processes an orthomosaic into a 2D footprint map. Orthomosaics that have been georeferenced allow for the generation of maps with proper scale and orientation. Cross sections from the 3D model can then be placed around the map to add information on the cave's interior features.

While this cave was not georeferenced, there was still an opportunity to evaluate accuracy and potential drift by comparing it to the pre-existing survey sketch from 1994. The trend of the cave walls matched fairly closely with the older cave sketch, but had some deviations such as in the width of the U-shaped bend in the central part of the model. Because of

this, the cave was resurveyed in 2016. To avoid any bias, the cave sketch was not drawn by the author. Analyzing all three representations of the cave quickly reveals that all three characterize the cave in a highly similar but unique fashion. The 1994 sketch clearly differs in several areas from the 2016 sketch, which underlines the highly subjective nature of hand drawing the shape of the walls. Unfortunately, it cannot be said with great confidence whether one representation or the other is "more correct" only that they all do not agree 100% with each other. A side by side comparison of the three different cave maps is offered in Figure 26.

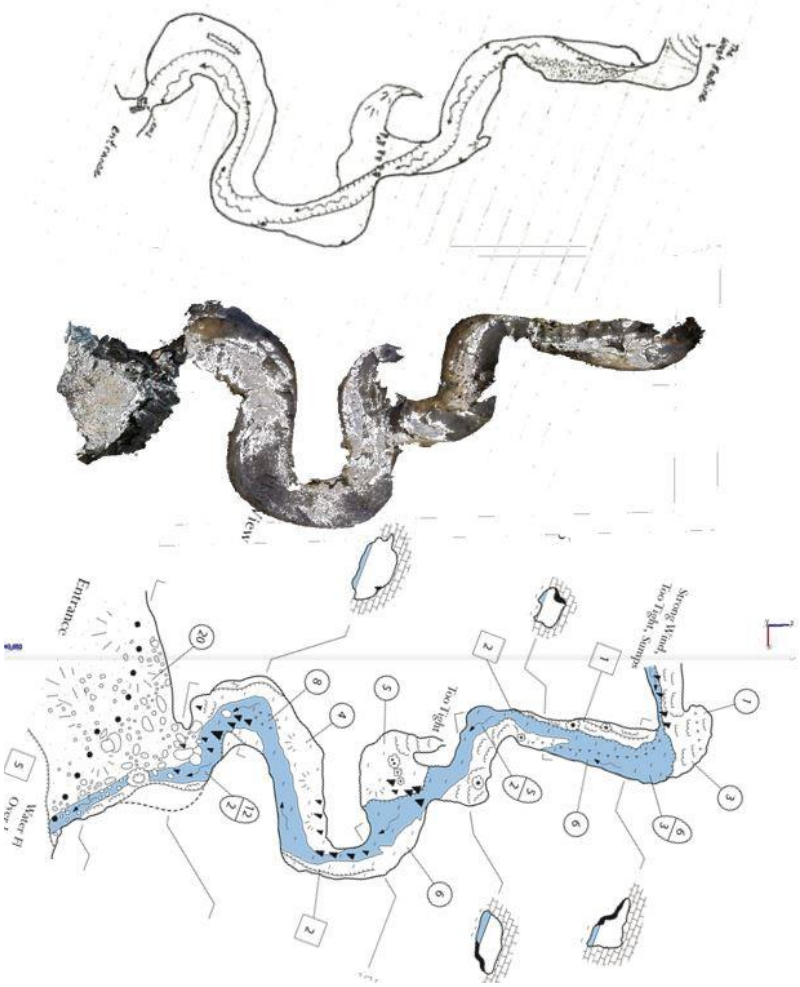

Fig 26. Original 1994 compass and tape survey by W.Pierce and K. McCormick at top, photogrammetric survey in middle, and newer 2016 compass and Disto survey by Kayla Sapkota and Joseph Jordan on bottom. Sketching and cartography was completed independently by Kayla Sapkota to ensure there was no bias introduced from the author.

5.5 University of Arkansas Utility Tunnels

While not a true natural cave, the university utility tunnels offered a unique opportunity to test the method in a manmade subterranean structure with a straight line overall trend and straight vertical supports along the corridor. While minor distortions in natural random cave wall geometry would be difficult to spot, here, any curved passage or warped support beams would immediately represent error in the method. Approximately 30m of the tunnel was modeled with the primary goal of observing any distortion or deviation in the predictable manmade corridor. Other objectives of the project included comparing several types of control targets and testing the use of split frames in a video opposed to still images.

It was immediately apparent during image acquisition that there was a large amount of distortion in the image from the fisheye lens. The vertical support beams looked normal from a distance but gradually became more and more distorted as the camera approached them. The severity of this distortion at its greatest is illustrated in Figure 27.

Fig 27. Severely distorted vertical support in the utility tunnel.

Luckily this distortion did not carry over into the 3D model. Both the video method and the still frame method successfully captured the straight-line trend of the tunnel, and rather than constructing warped vertical beams, these were simply removed by the software, automatically. Additionally, both models captured the slight downward slope to the drain and the slight upward slope of the tunnel after the drain, which were nearly imperceptible to the human eye in the images. Although the overall trend of the structure was good, the quality of the mesh in both models was undesirable containing numerous holes as well as an "acid eaten" texture to the surface. This was partially remedied through the use of the PhotoScans "smooth mesh" tool, but consequently lead to a loss of detail and sharpness, especially notable by a slight distortion in the two tripod mounted targets set up in the tunnel. Even after the smoothing, pipes and walls in both models had a mangled appearance. It is likely that the complexity of various supports and pipes running across the walls made this environment difficult to model as the camera could not see all the different sides of these objects. The camera also could not image what was behind these objects leading to periodic holes in the side walls of the corridor. Post it notes, tripod mounted targets, and printable coded targets from PhotoScan were all tested in this model. Unfortunately, the post it notes were placed on the vertical supports which were automatically removed from the model, so these could not be evaluated. The tripod mounted targets offered good 3D targets, but were distorted by the mesh smoothing tool. Coded targets worked the best, and it was discovered that the software can scan for and detect these targets automatically even before the photo alignment step. Six of these markers were placed on the floor, while two of them were placed on the wall. Though all six floor targets were detected and clearly modeled in both the video frame and still image tests, only one of the side wall targets was detected in the video frame test. This target was severely distorted.

The last part of this experiment plotted the same section of passage captured with still photos vs a video split into individual frames and evaluated the models on several different aspects. The video was made using the 1080p 60 fps setting with low light mode turned on.

With still images, the corridor took 81 images to model, which were all processed in one chunk. Because these two models were processed in Agisoft version 1.2.6, details were recorded on the exact time each step took to process. For this first model, total processing time was about 1 hour and 35 min. The finished model consisted of 42,542 tie points, 9,479,861 points in the dense cloud, and a mesh model containing 631,989 faces. RMS re-projection error was 1.49 pixels, while max re-projection error was 55.32 pixels. The effective overlap value for the model was 2.74. The plan view of the model looks correct with a few small floating chunks of mesh along the left side. It took around 15-20 min to take the 81 photos. A screen capture looking down the model is presented in Figure 28.

Fig 28. View looking down model created with still images

The other was created using 200 individual video frames. Despite the larger number of images, this model processed faster with an overall processing time of 1 hour and 9 minutes. At 58,758 the model had more tie points, but less than half of the number of total points and faces at just 4,083,041 and 257,741 respectively. According to the Agisoft report the model had less re-projection error at an RMSE re-projection of 1.23 pixels, and a maximum re-projection error of 25.19 pixels. This model also, as expected, had a higher effective overlap value of 3.21. Despite this however, this model contained more error visually, with several significant bulges along the exterior of the left wall, most severe of which is in the central part of the model. Internally, the quality of the mesh was similar, with a much lighter appearance to the textured mesh model most likely due to the low light mode that was used during video capture. The video frames seem to be lower resolution, less in focus than the still photos, and lack the EXIF data containing camera specification used in the calibration process. All of this was accomplished however at a fraction of the time, only a two to three minutes of steadily walking down the passage in video mode. It is also important to consider that consistent movement speed was easy walking down the tunnel, but would be more difficult in many cave environments. It's likely that there would be a great deal of excess video footage (and frames) through highly confined passages or those containing difficult obstacles. A screen capture looking through the tunnel model generated with the video method is presented in Figure 29. More detailed information on each cave model as well as a plan view of the models can be found in the appendix.

Fig 29. Model generated with individual frames split from continuous GoPro video.

6. Conclusion

6.1 Research Question

The first objective of this research was to ascertain under what if any conditions can pure stand-alone photogrammetry be used to create interpretable 3D models of interior cave structures? This study concludes that using a bright floodlight and still images from a wide angle fisheye lens camera can in fact produce interpretable 3D models of underground cave structures. The use of split frames from a video camera was also established as a comparable method, allowing a faster scanning speed and greater image overlap at the cost of lower resolution and possibly lower accuracy. The most successful environmental conditions were those where the lowest part of the floor, the width of the walls, and the vertical extent of the ceiling were clearly illuminated and unobstructed by any interior features. The methodology worked best in cave passages less than 10.6 meters (35 feet) wide, with consistent ceiling height, minimal standing

water on the floor, and no complex structures lining the side walls. Agisoft PhotoScan was the software of choice for producing the models utilizing the ability to isolate tricky areas in individual chunks and later merge then together into complete cave models. Disabling pair pre-selection among several other processing settings and parameters were critical to the successful construction of the models.

A secondary goal of the research was to evaluate the accuracy of the generated models with respect to currently held cave survey accuracy standards. Plan views of the 3D models agreed for the most part with traditional cave sketches. Although there were some small deviations between the cave sketch of Dogwood Cave and the corresponding 3D model, the two sketches of this cave from different years also did not agree completely with each other.

The accuracy of measurements made in the model depends heavily on the quality of the control network used to georeference it. In this case of Birch Cave, real world measurements typically agreed with measurements in the virtual model within a meter. As reported by the PhotoScan report, the control network had a total error of 1.2 meters. The RMSE projection error was typically between 1-2 pixels, while the max re-projection error ranged from 25.19 to 84.07 pixels in the largest model in Birch Cave. In reference to the BCRA cave accuracy standards, the survey line used achieves Grade 4 accuracy, where all angles agree within 2 degrees, distances were measured with the Disto which is accurate to 1.5875 mm(1/16 of an inch), and exact station locations in the model were definable within a radius of a few centimeters. The highest rating for cave passage detail is Class D and is defined by "measurements of detail made at survey stations and wherever else needed to show significant changes in passage dimensions" ("BCRA Survey Grades", 2002). Since in this case every vertex in the cave walls was measured by the software, the method used technically surpasses Class D

in accuracy. However, this assumes that the photogrammetrically derived measurements between stations and at all critical points of change in the model are to the same accuracy. In either case, the cave wall geometry constructed by the photogrammetric method largely agrees with traditional cave sketches where cave walls were interpretively drawn between stations as the caver eye-balled them. It can be said that the result of the photogrammetric method at the very least achieves a similar accuracy to that of the human, hand drawn interpretations of the cave.

6.2 Real World Applications

The methodology discussed in this paper allows for cave survey to move beyond the 2D sketch map to capture the entirety of subterranean structures, and any notable features they contain. Accurate scale and orientation still relies on a survey line traverse, but eliminates the need to hand sketch cave walls, ledges, profiles, cross sections, and internal features.

It is the opinion of the author that in its present highly experimental state, the proposed methodology should not replace traditional cave survey, but that it is a valuable supplement to it. Photogrammetric models, under ideal conditions, capture more of the cave than a 2D map can and do so using inexpensive, cave friendly equipment that is easy to use. Finished models can be used to study speleogensis as well as cave morphology especially in the analysis of the size and location of scallops. These models can be converted into caving simulations and virtual tours that can be used for education and outreach to people who are not willing or able to physically travel to or explore the caves. With further research and advancement in the technology, this system could also be used as an effective low budget strategy for the modeling of mining operations, municipal storm water drainage systems (MS4s), and utility tunnels.

6.3 Future Research Areas

Numerous ideas and questions came about as a result of the experiments discussed in this paper. Though these were out of the scope of this paper, they may represent important topics for future studies.

In theory, the wide angle fisheye lens is a huge part of what makes this method possible, as each picture captures much more information about the environment than a conventional frame camera. However, this is speculative and yet to be proven. An imitation of this research with a variety of camera types would be beneficial in establishing concrete evidence supporting the degree to which camera and lens type matter for the application of capturing 3D tunnels and passageways. It is possible that different cameras, settings, and light rigs could achieve better results than those achieved in this project.

The accuracy assessment of traverse data and control networks is not critically important, because these are widely used and mature methods that are used both in traditional and photogrammetric cave survey. More important, is an assessment of the geometry of the cave walls generated by the photogrammetric method, and how close they represent the walls in reality. In this research, photogrammetric models were roughly compared to the hand drawn cave maps that were available. The problem is that those hand drawn cave maps used as a control cannot be proven to be any more accurate than the models. A better assessment of relative accuracy would be to directly compare the CRP method to a TLS survey and analyze the point clouds and any deviation in terms of their Hausdorf distance.

In retrospect, after this work was completed, it was noted that the PhotoScan camera calibration parameters were set to the "frame" setting instead of "fisheye." It would be valuable,

in future research, to examine various calibration methods and models and examine whether or not they lead to significant changes in the final products and their accuracy.

The only equipment needed to repeat this method is a light source and a GoPro camera. The simplicity in this system is significant in that it could potentially be mounted to a small unmanned remote control vehicle for the exploration and 3D mapping of tight passages that are too tight for humans. With enough light, the method should theoretically work the same underwater, allowing for a remote control submersible vehicle to explore sumps and flooded cave passages. Finally, the same could be done with a quadcopter or other UAV system for use in 3D modeling large vertical pits.

References

Addison A., (2011). LiDAR at Mammoth Cave. *Civil Engineering Surveyor,* (April 2011) 22-25

Agisoft LLC. (2016). *Agisoft PhotoScan User Manual; Professional Edition version 1.2*

BCRA Survey Grades. (2002, November 10). Retrieved from http://bcra.org.uk/surveying/

Brown, K. R., Chalmers, A., Saigol, T., Green, C., & D'errico, F. (2001). An Automated Laser Scan Survey of the Upper Paleolithic Rock Shelter of Cap Blanc. *Journal of Archaeological Science*, *28*(3), 283-289.

Buchroithner, M. F., & Gaisecker, T. (2009). Terrestrial Laser Scanning for the Visualization of a Complex Dome in an Extreme Alpine Cave System. *Photogrammetrie - Fernerkundung - Geoinformation*, *2009*(4), 329–339. https://doi.org/10.1127/1432-8364/2009/0025

Caprioli, M., Minchilli, M., Scognamiglio, A., & Strisciuglio, G. (2003). Using photogrammetry and laser scanning in surveying monumental heritage: le Grotte di Castellana. *International Archives of Photogrammetry Remote Sensing and Spatial Information Sciences*, *34*(5/W12), 107–110.

Chandler, J. H., & Fryer, J. G. (2005). Recording aboriginal rock art using cheap digital cameras and digital photogrammetry. Retrieved from https://dspace.lboro.ac.uk/dspace/handle/2134/2240

Cooper, S. E., (1998*). Softcopy Photogrammetry and the Development of Field Methodologies Applied to the Recording and Analysis of Rock Art* (Masters Thesis). University of Arkansas Special Collection Storage. (T 1998 C664 Archival Copy)

Dasher, G. R. (1994). On Station: A Complete Handbook for Surveying and Mapping Caves. Huntsville (AL): National Speleological Society. 240 p. Quote excerpt from p. 42.

El-Hakim, S. F., Fryer, J. G., & Picard, M. (2004). Modelling and Visualization of Aboriginal Rock Art in the Baiame Cave. *International Archives of Photogrammetry and Remote Sensing*, *35*(5), 990–995.

Furukawa, Y. (2013). Multi-view Stereo: A Tutorial. *Foundations in Computer Graphics and Vision, 9*(1-2), 3-14.

Ghosh, S. K., (1981). History of Photogrammetry -Analytical Methods and Instruments. *XVIIth ISPRS Congress Proceedings--Technical Commission VI: Economic, Professional and Educational Aspects of Photogrammetry and Remote Sensing*, 29, 311-327.

González-Aguilera, D., Muñoz-Nieto, A., Gómez-Lahoz, J., Herrero-Pascual, J., & Gutierrez-Alonso, G. (2009). 3D Digital Surveying and Modelling of Cave Geometry: Application to Paleolithic Rock Art. *Sensors*, *9*(2), 1108–1127. https://doi.org/10.3390/s90201108

González-Aguilera, D., Muñoz-Nieto, A., Picon-Cabrera, I., Gomez-Lahoz, J., Herrero-Pascual, J., Mancera-Taboada, J., & Rodriguez-Gonzálvez, P. (2011). *Application of non-*

destructive techniques to the recording and modelling of palaeolithic rock art. INTECH Open Access Publisher. Retrieved from http://cdn.intechweb.org/pdfs/15812.pdf

Grussenmeyer, P., & Jasmine, J. (2003). The Restoration of Beaufort Castle (South-Lebanon): A 3D Restitution According to Historical Documentation. In *XIXth CIPA International Symposium*, (pp. 322–327). Retrieved from https://halshs.archives-ouvertes.fr/halshs-00264004/

Grussenmeyer, P., Landes, T., Alby, E., Carozza, L., (2010). High Resolution 3D Recording and Modelling of the Bronze Age Cave "Les Fraux" in Perigord (France). *International Archives of Photogrammetry, Remote Sensing, and Spatial Information Sciences, Vol 38*(5) 262-267.

Grussenmeyer, P., Alby, E., Landes, T., Koehl, M., Guillemin, S., Hullo, J., & Smigiel, E. (2012). Recording Approach of Heritage Sites Based on Merging Point Clouds from High Resolution Photogrammetry and Terrestrial Laser Scanning. *Int. Arch. Photogramm. Remote Sens. Spat. Inf. Sci*, *34*, 553–558.

Hero 3+ Black Edition Field of View Information. (n.d.). Retrieved from https://gopro.com/support/articles/hero3-field-of-view-fov-information

Higgins, Sean. (2015, March 04). *Fisheye Lenses Make the Impossible Possible.* Retrieved from http://www.spar3d.com/blogs/the-other-dimension/vol13no9-fisheye-lenses-make-the-impossible-possible/

Higgins, Sean (2016, November 16). *Meet Leicas 16k LiDAR scanner, the BLK360*. Retrieved from http://www.spar3d.com/news/lidar/meet-leicas-16k-scanner-blk360/

Howard, I. P., Brian, R., J. (2012). *Perceiving in Depth, Volume 2: Stereoscopic Vision.* New York, NY: Oxford University Press.

Hudson, M. R., Turner, K. J., & Bitting, C. (2011). Geologic Framework of Karst Features in Western Buffalo National River, Northern Arkansas. *US Geological Survey Karst Interest Group Proceedings, Fayetteville, Arkansas, April 26–29, 2011*, 16-17.

Huttenlocher, D., Klanderman, G. A., & Rucklidge, W. J., (1993). Comparing Distances Using the Hausdorff Distance. *IEEE Transactions on Pattern Analysis and Machine Intelligence, 15*(9) 850-862.

Idrees, O.M., & Pradhan B., (2016). A Decade of Modern Cave Surveying with Terrestrial Laser Scanning. A Review of Sensors, Method, and Application Development. *International Journal of Speleology, 45*(1) ,71-88. Tampa, FL ISSN 0392-6672.

Kolecka, N., (2011). Photo-based 3D Scanning vs. Laser Scanning-Competitive Data Acquisition Methods for Digital Terrain Modelling of Steep Mountain Slopes. ISPRS - International Archives of the Photogrammetry, Remote Sensing and Spatial Information Sciences, 38(-4/W19) 203-208.

Lerma, J. L., Navarro S., Cabrelles, M., & Villaverde, V. (2010). Terrestrial Laser Scanning and Close Range Photogrammetry for 3D Archaeological Documentation: the Upper Palaeolithic Cave of Parpalló as a Case Study. *Journal of Archaeological Science, 37,* 499-507.

Lingua, A., Marenchino, D., & Nex, F. (2009). Performance Analysis of the SIFT Operator for Automatic Feature Extraction and Matching in Photogrammetric Applications. *Sensors*, *9*(05), 3745-3766.

McCormac, Jack. (2004) *Surveying*. Hoboken, NJ: Wiley.

McFarlane, D. A., Buchroithner, M., Lundberg, J., Petters, C., Roberts, W., & Van Rentergen, G. (2013). Integrated three-dimensional laser scanning and autonomous drone surface-photogrammetry at Gomantong caves, Sabah, Malaysia. In *Proceedings of the 16th International Congress of Speleology, Brno* (Vol. 1, pp. 317–319). Retrieved from https://www.researchgate.net/profile/Manfred_Buchroithner/publication/261097340_Gomantong_Congress_Paper_2013/links/00b7d5332d8cf3bd16000000.pdf

Milius, J., & Petters, C. (2012). Eisriesenwelt–From laser scanning to photo-realistic 3D model of the biggest ice cave on Earth. In *GI-Forum* (pp. 513-523).

Moreno, A., G., & Garate, D., 2012. Low-Cost Photogrammetry and 3D scanning: the Documentation of Paleolithic Parietal Art in El Niño Cave. *CAA2012 Proceedings of the 40th Conference in Computer Applications and Quantitative Methods in Archaeology, Southampton, United Kingdom, 26-30 March 2012*, p. 344-348.

Núñez, M. A., Buill, F., & Edo, M. (2013). 3D model of the Can Sadurní cave. *Journal of Archaeological Science*, *40*(12), 4420–4428. https://doi.org/10.1016/j.jas.2013.07.006

Matthews, N., A. (2008). *Aerial and Close-Range Photogrammetric Technology: Providing Resource documentation, Interpretation, and Preservation.* Technical Note 428. U.S Department of Interior, Bureau of Land Management, National Operations Center, Colorado. P42.

Positional Accuracy. (2003, February 24). Retrieved from http://www.gitta.info/MetaDataQual/en/html/PositAccurac_learningObject1.html

Roncat, A., Dublyansky, Y., SpöTl, C., & Dorninger, P. (2011). *Full-3D Surveying of Caves: A Case Study of Märchenhöhle (Austria)*. cogeo@oeaw-giscience. https://doi.org/10.5242/iamg.2011.0074

Rüther, H., Chazan, M., Schroeder, R., Neeser, R., Held, C., Walker, S. J., & Horwitz, L. K. (2009). Laser scanning for conservation and research of African cultural heritage sites: the case study of Wonderwerk Cave, South Africa. *Journal of Archaeological Science*, *36*(9), 1847–1856. https://doi.org/10.1016/j.jas.2009.04.012

Schwinge, H. T., (1962). The Accuracy of Cave Survey. *Bulletin of the National Speleological Society, 24*, 40-47

Thrun, R., (2000). A Statistical Study of Survey Errors and Closure Adjustments. *2000 NSS convention.* Revised in 2009.

Urban, S., & Hinz, S. (2016). MultiCol-SLAM-A Modular Real-Time Multi-Camera SLAM System. arXiv Preprint arXiv:1610.07336. Retrieved from https://arxiv.org/abs/1610.07336

Westoby, M. J., Brasington, J., Glasser, N. F., Hambrey, M. J., & Reynolds, J. M. (2012). 'Structure-from-Motion'photogrammetry: A low-cost, effective tool for geoscience applications. *Geomorphology*, *179*, 300-314.

Appendix A: PhotoScan Processing Reports

Aspen Cave

Processing Report
05 April 2017

Survey Data

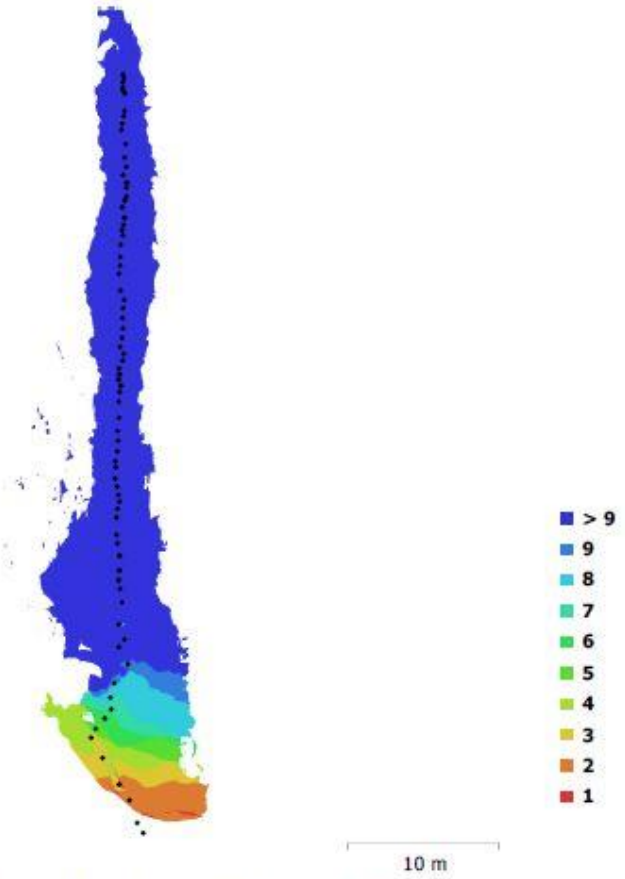

Fig. 1. Camera locations and image overlap.

Number of images:	87	Camera stations:	87
Flying altitude:	3.74 m	Tie points:	19,944
Ground resolution:	1.52 mm/pix	Projections:	72,049
Coverage area:	256 m²	Reprojection error:	1.13 pix

Camera Model	Resolution	Focal Length	Pixel Size	Precalibrated
HERO3+ Black Edition (2.77 mm)	4000 x 3000	2.77 mm	1.6 x 1.6 µm	No
HERO3+ Black Edition (2.77 mm)	4000 x 3000	2.77 mm	1.6 x 1.6 µm	No
HERO3+ Black Edition (2.77 mm)	4000 x 3000	2.77 mm	1.6 x 1.6 µm	No

Camera Calibration

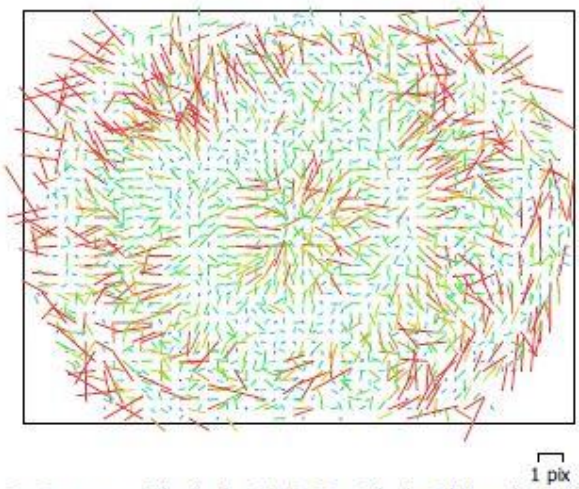

Fig. 2. Image residuals for HERO3+ Black Edition (2.77 mm).

HERO3+ Black Edition (2.77 mm)

20 images

Type	Resolution	Focal Length	Pixel Size
Frame	**4000 x 3000**	**2.77 mm**	**1.6 x 1.6 µm**
F:	1765.15		
Cx:	-19.973	B1:	0
Cy:	20.7287	B2:	0
K1:	-0.24195	P1:	0
K2:	0.0683675	P2:	0
K3:	-0.00896325	P3:	0
K4:	0	P4:	0

Camera Calibration

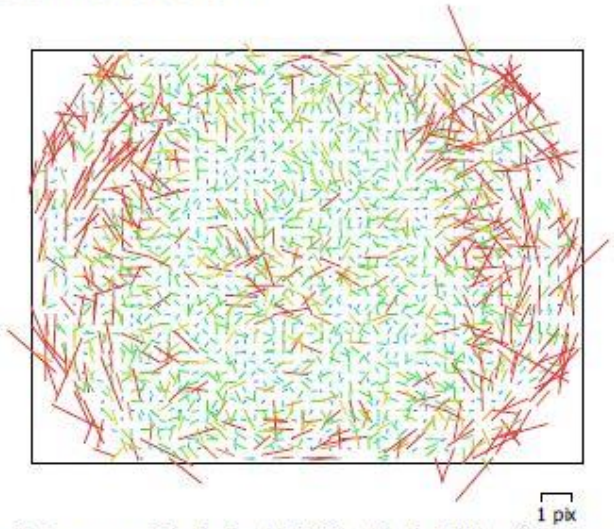

Fig. 3. Image residuals for HERO3+ Black Edition (2.77 mm).

HERO3+ Black Edition (2.77 mm)

23 images

Type	Resolution	Focal Length	Pixel Size
Frame	**4000 x 3000**	**2.77 mm**	**1.6 x 1.6 µm**
F:	1791.8		
Cx:	-27.1135	B1:	0
Cy:	19.8895	B2:	0
K1:	-0.230227	P1:	0
K2:	0.0587987	P2:	0
K3:	-0.00675683	P3:	0
K4:	0	P4:	0

Camera Calibration

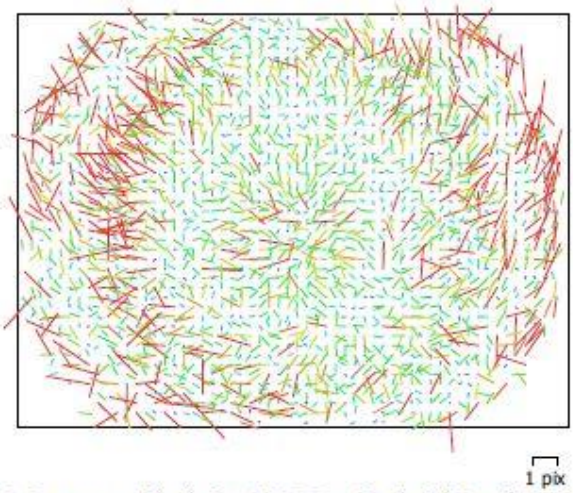

Fig. 4. Image residuals for HERO3+ Black Edition (2.77 mm).

HERO3+ Black Edition (2.77 mm)

23 images

Type	Resolution	Focal Length	Pixel Size
Frame	**4000 x 3000**	**2.77 mm**	**1.6 x 1.6 µm**
F:	1770.52		
Cx:	-30.9809	B1:	0
Cy:	35.75	B2:	0
K1:	-0.236832	P1:	0
K2:	0.0645995	P2:	0
K3:	-0.00796939	P3:	0
K4:	0	P4:	0

Camera Calibration

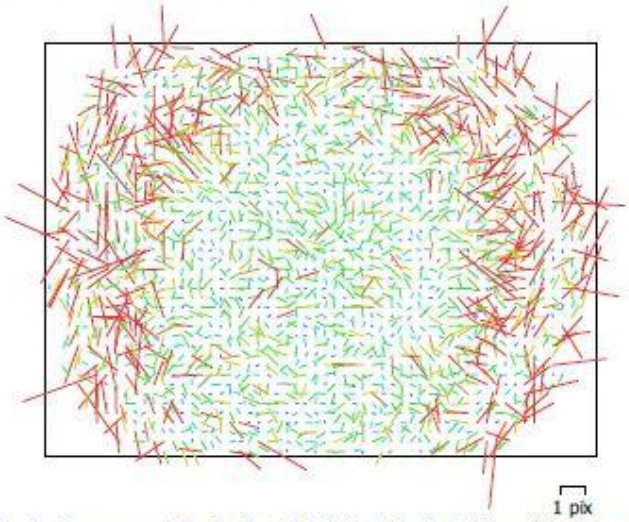

Fig. 5. Image residuals for HERO3+ Black Edition (2.77 mm).

HERO3+ Black Edition (2.77 mm)

21 images

Type	Resolution	Focal Length	Pixel Size
Frame	**4000 x 3000**	**2.77 mm**	**1.6 x 1.6 µm**

F:	1773.69		
Cx:	-15.9907	B1:	0
Cy:	36.3544	B2:	0
K1:	-0.24043	P1:	0
K2:	0.0678989	P2:	0
K3:	-0.00898094	P3:	0
K4:	0	P4:	0

Digital Elevation Model

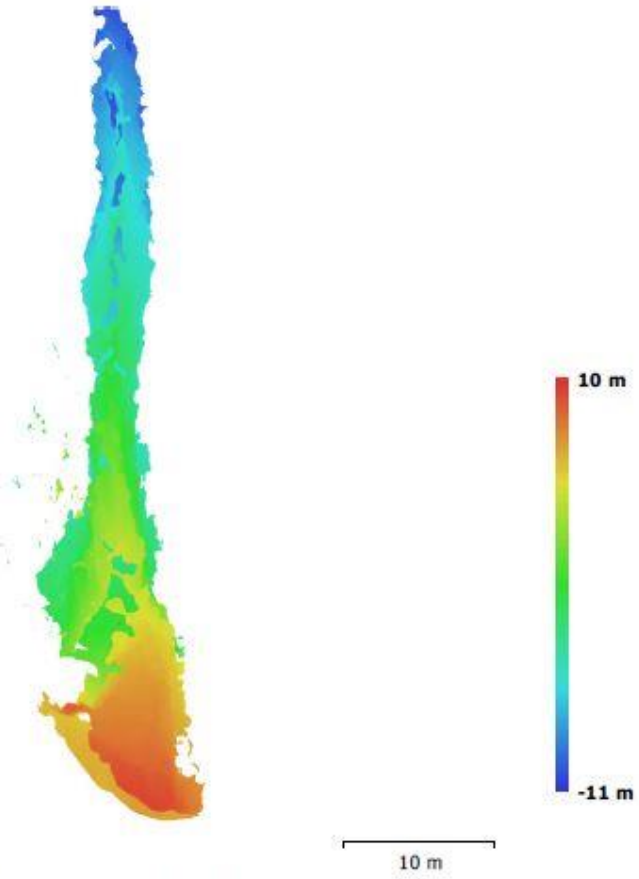

Fig. 6. Reconstructed digital elevation model.

Resolution:	6.07 mm/pix
Point density:	2.72 points/cm²

Processing Parameters

General	
Cameras	87
Aligned cameras	87
Coordinate system	Local Coordinates (m)
Rotation angles	Yaw, Pitch, Roll
Point Cloud	
Points	19,944 of 23,781
Reprojection error	1.12701 (3.63269 max)
Effective overlap	3.79429
Dense Point Cloud	
Points	15,502,011
Reconstruction parameters	
Quality	Medium
Depth filtering	Aggressive
Model	
Faces	1,037,796
Vertices	527,322
Texture	4,096 x 4,096, uint8
Reconstruction parameters	
Surface type	Arbitrary
Source data	Dense
Interpolation	Enabled
Quality	Medium
Depth filtering	Aggressive
Texturing parameters	
Mapping mode	Generic
Blending mode	Mosaic
Texture size	4,096 x 4,096
Enable color correction	No
Enable hole filling	Yes
UV mapping time	1 minutes 17 seconds
Blending time	4 minutes 3 seconds
Software	
Version	1.3.0 build 3772
Platform	Windows 64

Birch Cave

Processing Report
05 April 2017

Survey Data

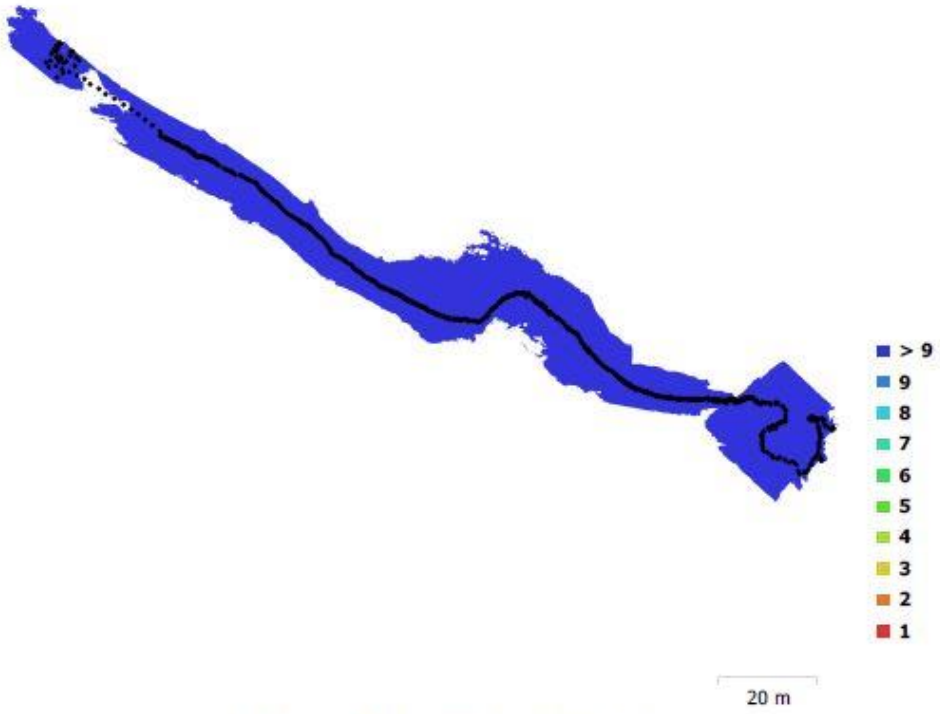

Fig. 1. Camera locations and image overlap.

Number of images:	678	Camera stations:	678
Flying altitude:	4.27 m	Tie points:	151,239
Ground resolution:	1.64 mm/pix	Projections:	494,053
Coverage area:	2.24e+03 m²	Reprojection error:	2.57 pix

Camera Model	Resolution	Focal Length	Pixel Size	Precalibrated
HERO3+ Black Edition (2.77 mm)	4000 x 3000	2.77 mm	1.6 x 1.6 µm	No
HERO3+ Black Edition (2.77 mm)	4000 x 3000	2.77 mm	1.6 x 1.6 µm	No
HERO3+ Black Edition (2.77 mm)	4000 x 3000	2.77 mm	1.6 x 1.6 µm	No

Camera Model	Resolution	Focal Length	Pixel Size	Precalibrated
HERO3+ Black Edition (2.77 mm)	4000 x 3000	2.77 mm	1.6 x 1.6 µm	No
HERO3+ Black Edition (2.77 mm)	4000 x 3000	2.77 mm	1.6 x 1.6 µm	No
HERO3+ Black Edition (2.77 mm)	4000 x 3000	2.77 mm	1.6 x 1.6 µm	No
HERO3+ Black Edition (2.77 mm)	4000 x 3000	2.77 mm	1.6 x 1.6 µm	No

Table 1. Cameras.

Camera Calibration

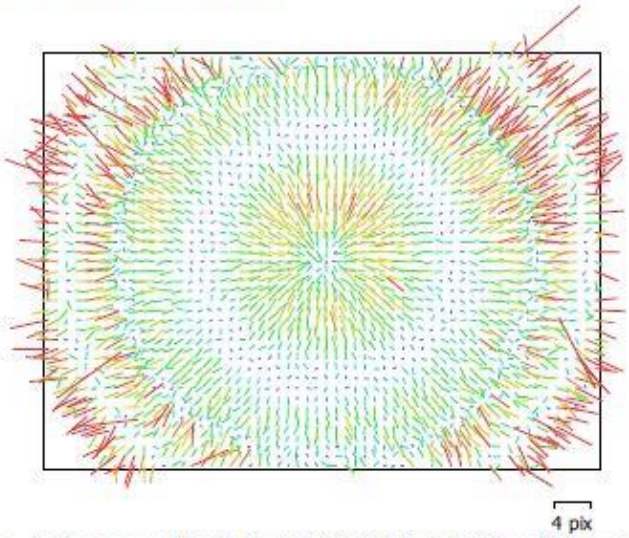

Fig. 2. Image residuals for HERO3+ Black Edition (2.77 mm).

HERO3+ Black Edition (2.77 mm)
144 images

Type	Resolution	Focal Length	Pixel Size
Frame	**4000 x 3000**	**2.77 mm**	**1.6 x 1.6 µm**
F:	1756.54		
Cx:	26.7091	B1:	0
Cy:	-20.9698	B2:	0
K1:	-0.222511	P1:	-0.000137648
K2:	0.051103	P2:	0.000252484
K3:	-0.00511228	P3:	0
K4:	0	P4:	0

Camera Calibration

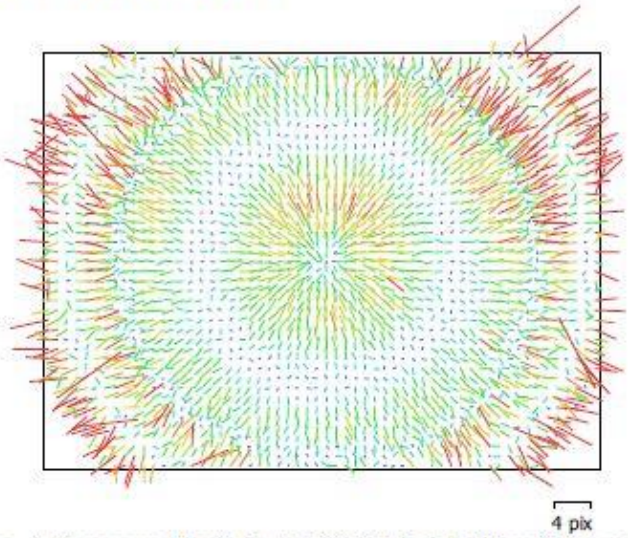

Fig. 2. Image residuals for HERO3+ Black Edition (2.77 mm).

HERO3+ Black Edition (2.77 mm)
144 images

Type	Resolution	Focal Length	Pixel Size
Frame	**4000 x 3000**	**2.77 mm**	**1.6 x 1.6 µm**
F:	1756.54		
Cx:	26.7091	B1:	0
Cy:	-20.9698	B2:	0
K1:	-0.222511	P1:	-0.000137648
K2:	0.051103	P2:	0.000252484
K3:	-0.00511228	P3:	0
K4:	0	P4:	0

Camera Calibration

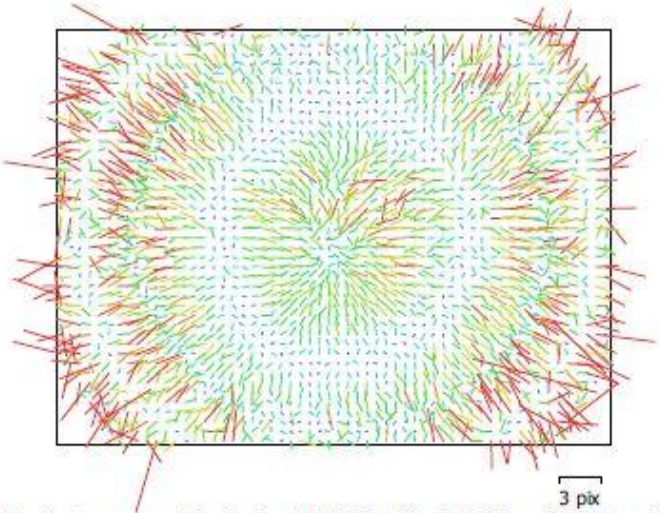

Fig. 3. Image residuals for HERO3+ Black Edition (2.77 mm).

HERO3+ Black Edition (2.77 mm)

141 images

Type	Resolution	Focal Length	Pixel Size
Frame	**4000 x 3000**	**2.77 mm**	**1.6 x 1.6 µm**

F:	1789.1		
Cx:	34.7211	B1:	0
Cy:	-14.8047	B2:	0
K1:	-0.224395	P1:	-0.000129246
K2:	0.0534509	P2:	0.000106967
K3:	-0.00560241	P3:	0
K4:	0	P4:	0

Camera Calibration

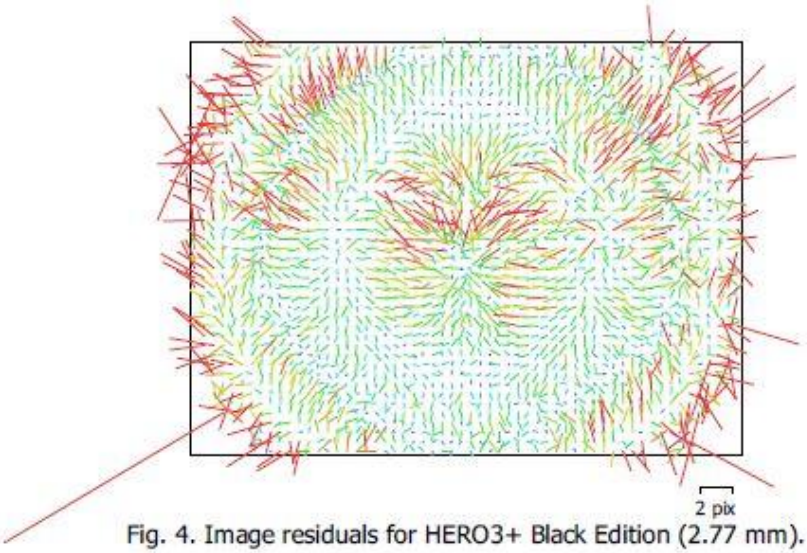

Fig. 4. Image residuals for HERO3+ Black Edition (2.77 mm).

HERO3+ Black Edition (2.77 mm)
107 images

Type	Resolution	Focal Length	Pixel Size
Frame	**4000 x 3000**	**2.77 mm**	**1.6 x 1.6 µm**

F:	1790.12		
Cx:	22.371	B1:	0
Cy:	-41.2637	B2:	0
K1:	-0.226323	P1:	-0.00033647
K2:	0.055689	P2:	0.000718489
K3:	-0.00616111	P3:	0
K4:	0	P4:	0

Camera Calibration

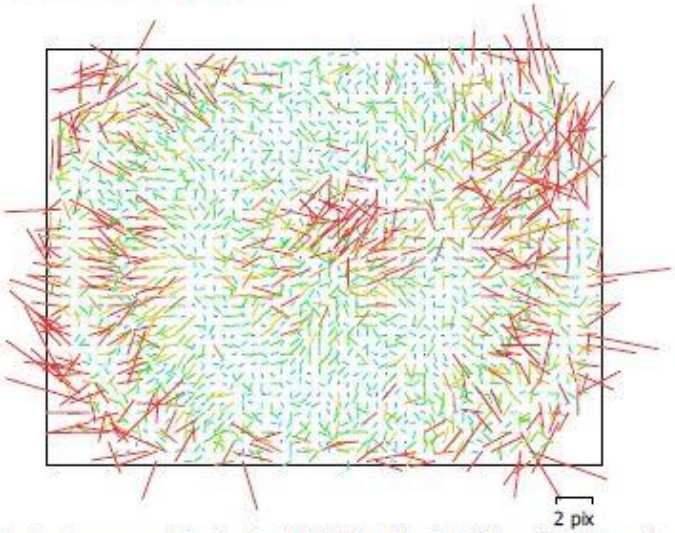

Fig. 5. Image residuals for HERO3+ Black Edition (2.77 mm).

HERO3+ Black Edition (2.77 mm)

76 images

Type	Resolution	Focal Length	Pixel Size
Frame	**4000 x 3000**	**2.77 mm**	**1.6 x 1.6 µm**

F:	1781.06		
Cx:	12.1092	B1:	0
Cy:	-37.2272	B2:	0
K1:	-0.22513	P1:	-0.000350184
K2:	0.0538873	P2:	0.000485335
K3:	-0.0056706	P3:	0
K4:	0	P4:	0

Camera Calibration

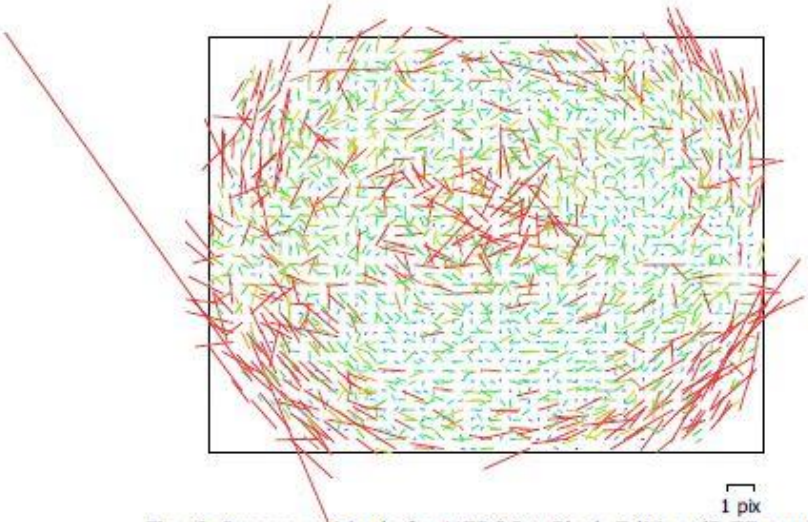

Fig. 6. Image residuals for HERO3+ Black Edition (2.77 mm).

HERO3+ Black Edition (2.77 mm)
62 images

Type	Resolution	Focal Length	Pixel Size
Frame	**4000 x 3000**	**2.77 mm**	**1.6 x 1.6 µm**

F:	1799.31		
Cx:	45.0917	B1:	0
Cy:	-38.0489	B2:	0
K1:	-0.220448	P1:	-3.62886e-05
K2:	0.0523828	P2:	0.000276348
K3:	-0.00562	P3:	0
K4:	0	P4:	0

Camera Calibration

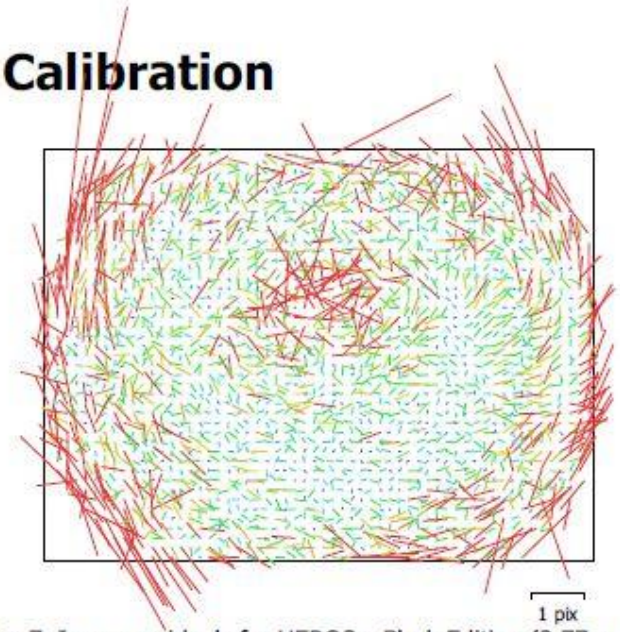

Fig. 7. Image residuals for HERO3+ Black Edition (2.77 mm).

HERO3+ Black Edition (2.77 mm)

73 images

Type	Resolution	Focal Length	Pixel Size
Frame	**4000 x 3000**	**2.77 mm**	**1.6 x 1.6 µm**
F:	1774.08		
Cx:	42.2392	B1:	0
Cy:	-50.8871	B2:	0
K1:	-0.221825	P1:	-0.000186885
K2:	0.0530352	P2:	0.000802454
K3:	-0.00564493	P3:	0
K4:	0	P4:	0

Camera Calibration

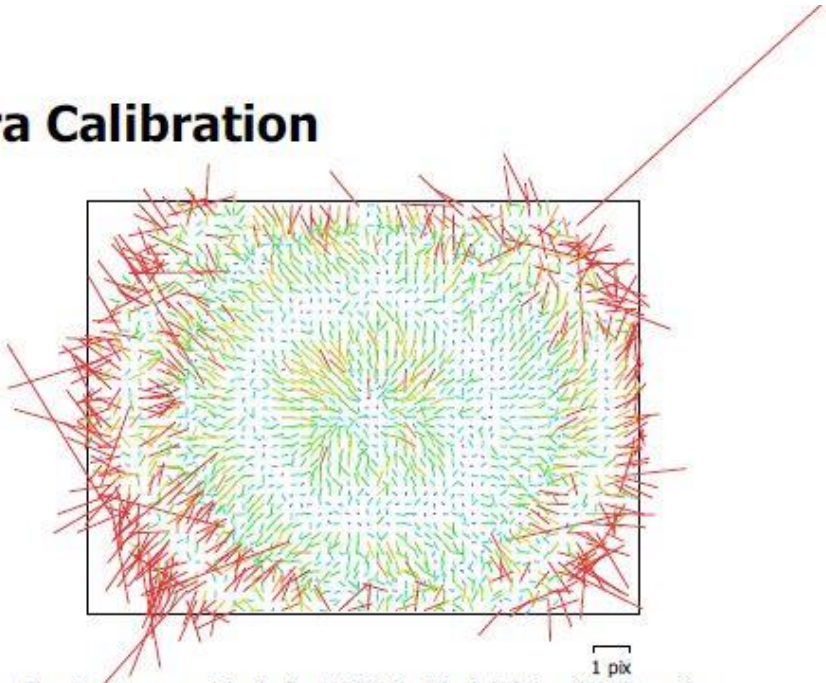

Fig. 8. Image residuals for HERO3+ Black Edition (2.77 mm).

HERO3+ Black Edition (2.77 mm)

75 images

Type	Resolution	Focal Length	Pixel Size
Frame	**4000 x 3000**	**2.77 mm**	**1.6 x 1.6 µm**

F:	1756.44		
Cx:	30.903	B1:	0
Cy:	-15.0911	B2:	0
K1:	-0.238853	P1:	-0.00020072
K2:	0.0652668	P2:	2.86982e-06
K3:	-0.00820423	P3:	0
K4:	0	P4:	0

Ground Control Points

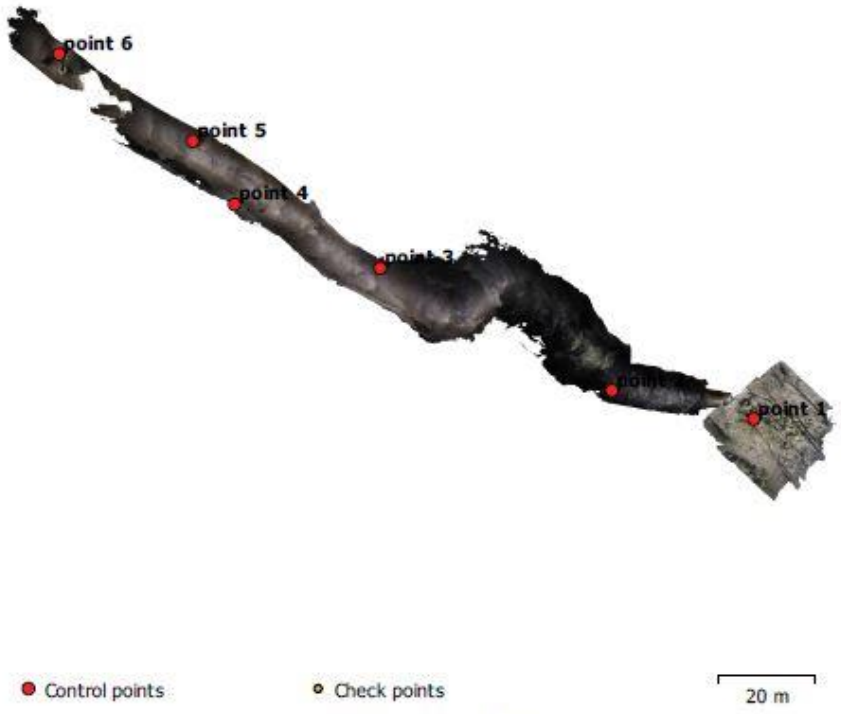

Fig. 9. GCP locations.

Count	X error (m)	Y error (m)	Z error (m)	XY error (m)	Total (m)
6	0.99285	0.434066	0.548633	1.08359	1.21456

Table 2. Control points RMSE.
X - Easting, Y - Northing, Z - Altitude.

Label	X error (m)	Y error (m)	Z error (m)	Total (m)	Image (pix)
point 1	1.47091	-0.125357	-0.292624	1.50496	0.000 (30)
point 2	-0.807128	-0.212727	0.930479	1.25	0.000 (120)
point 3	-1.26324	0.792292	-0.712222	1.6525	0.000 (158)
point 4	-0.479499	0.233919	-0.182537	0.563878	0.000 (105)
point 5	-0.0529091	-0.0679768	-0.246493	0.261111	0.000 (187)
point 6	1.12738	-0.618425	0.503222	1.38082	0.000 (239)
Total	**0.99285**	**0.434066**	**0.548633**	**1.21456**	**0.000**

Table 3. Control points.
X - Easting, Y - Northing, Z - Altitude.

Digital Elevation Model

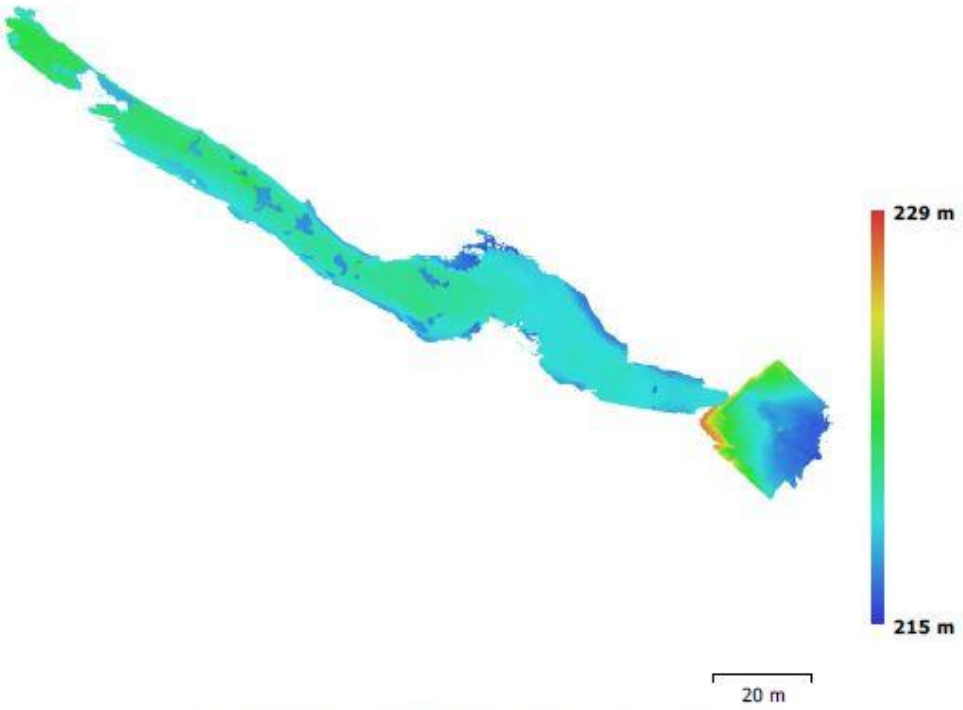

Fig. 10. Reconstructed digital elevation model.

Resolution:	6.56 mm/pix
Point density:	2.33 points/cm²

Processing Parameters

General	
Cameras	678
Aligned cameras	678
Markers	6
Coordinate system	NAD83 / Arkansas North (EPSG::26951)
Rotation angles	Yaw, Pitch, Roll
Point Cloud	
Points	151,239 of 227,895
RMS reprojection error	0.301872 (2.57434 pix)
Max reprojection error	4.23633 (84.0784 pix)
Mean key point size	8.54214 pix
Effective overlap	3.64514
Dense Point Cloud	
Points	66,782,453
Reconstruction parameters	
Quality	Medium
Depth filtering	Aggressive
Model	
Faces	4,435,017
Vertices	2,245,109
Reconstruction parameters	
Surface type	Arbitrary
Source data	Dense
Interpolation	Enabled
Quality	Medium
Depth filtering	Aggressive
Software	
Version	1.3.0 build 3772
Platform	Windows 64

Cedar Cave

Processing Report
05 April 2017

Survey Data

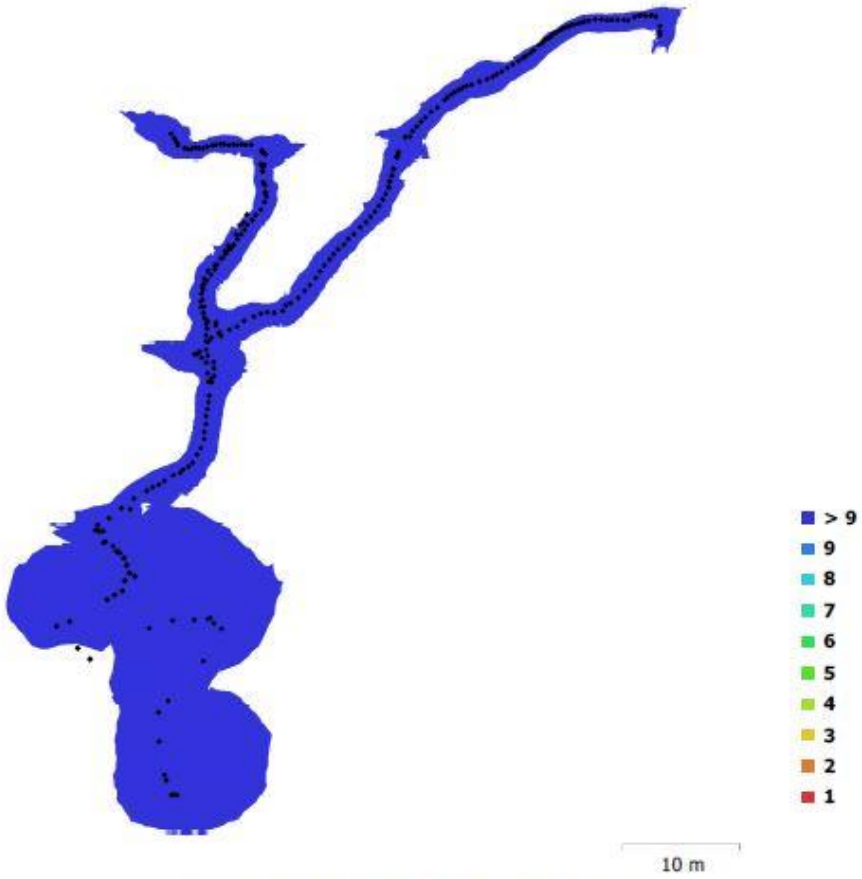

Fig. 1. Camera locations and image overlap.

Number of images:	425	Camera stations:	286
Flying altitude:	3.25 m	Tie points:	219,881
Ground resolution:	1.21 mm/pix	Projections:	583,279
Coverage area:	642 m²	Reprojection error:	1.23 pix

Camera Model	Resolution	Focal Length	Pixel Size	Precalibrated
HERO3+ Black Edition (2.77 mm)	4000 x 3000	2.77 mm	1.6 x 1.6 µm	No
HERO3+ Black Edition (2.77 mm)	4000 x 3000	2.77 mm	1.6 x 1.6 µm	No
HERO3+ Black Edition (2.77 mm)	4000 x 3000	2.77 mm	1.6 x 1.6 µm	No

Camera Calibration

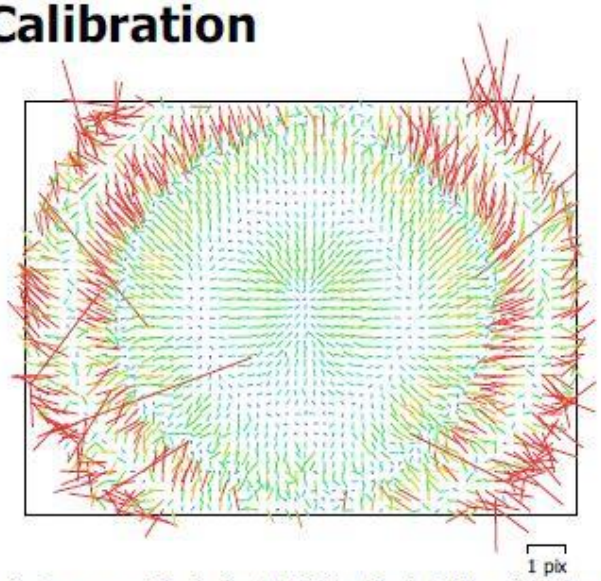

Fig. 2. Image residuals for HERO3+ Black Edition (2.77 mm).

HERO3+ Black Edition (2.77 mm)
296 images

Type	Resolution	Focal Length	Pixel Size
Frame	**4000 x 3000**	**2.77 mm**	**1.6 x 1.6 µm**

F:	1779.02		
Cx:	25.9099	B1:	0
Cy:	-22.1609	B2:	0
K1:	-0.239624	P1:	-0.000129857
K2:	0.0656569	P2:	0.000109616
K3:	-0.00818448	P3:	0
K4:	0	P4:	0

Camera Calibration

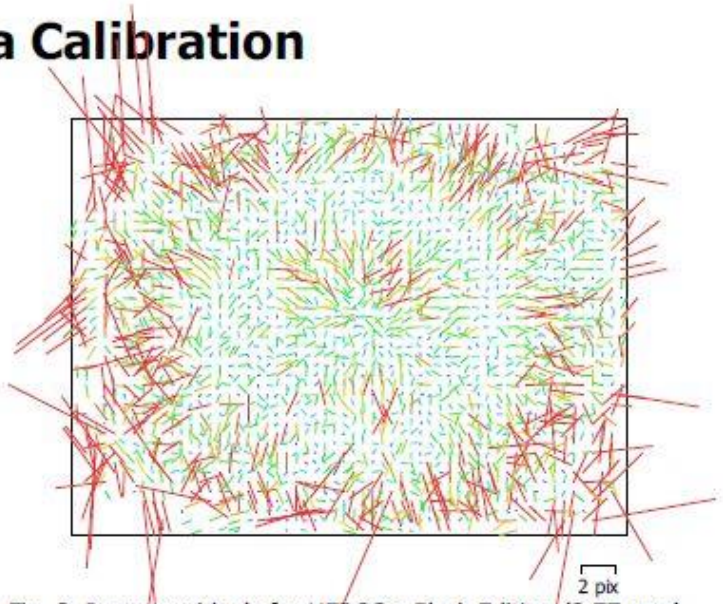

Fig. 3. Image residuals for HERO3+ Black Edition (2.77 mm).

HERO3+ Black Edition (2.77 mm)
28 images

Type	Resolution	Focal Length	Pixel Size
Frame	**4000 x 3000**	**2.77 mm**	**1.6 x 1.6 µm**
F:	1778.47		
Cx:	62.4122	B1:	0
Cy:	-41.6879	B2:	0
K1:	-0.222922	P1:	0.00045931
K2:	0.051009	P2:	0.000267499
K3:	-0.00490715	P3:	0
K4:	0	P4:	0

Camera Calibration

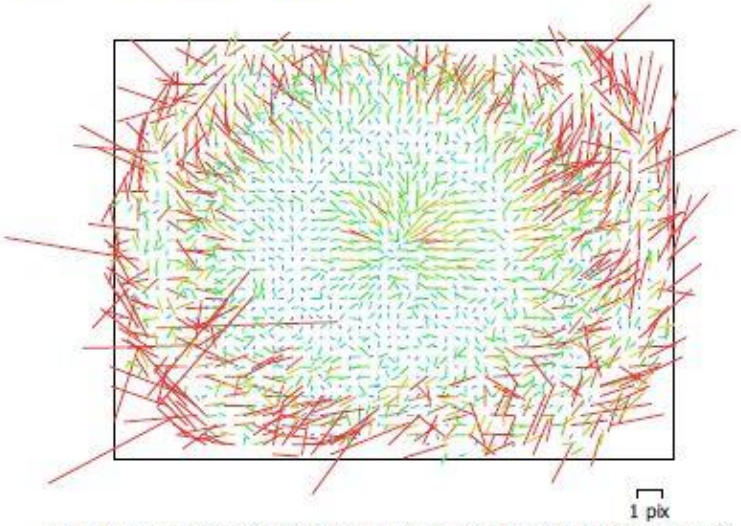

Fig. 4. Image residuals for HERO3+ Black Edition (2.77 mm).

HERO3+ Black Edition (2.77 mm)

31 images

Type	Resolution	Focal Length	Pixel Size
Frame	**4000 x 3000**	**2.77 mm**	**1.6 x 1.6 µm**

F:	1770.74		
Cx:	27.6798	B1:	0
Cy:	-18.3297	B2:	0
K1:	-0.238142	P1:	-0.000211211
K2:	0.0640686	P2:	7.06992e-05
K3:	-0.00779979	P3:	0
K4:	0	P4:	0

Camera Calibration

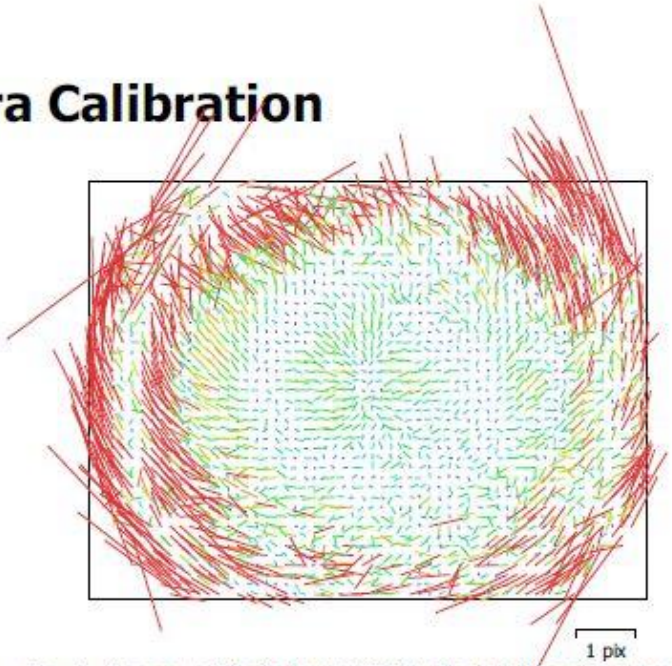

Fig. 5. Image residuals for HERO3+ Black Edition (2.77 mm).

HERO3+ Black Edition (2.77 mm)
70 images

Type	Resolution	Focal Length	Pixel Size
Frame	**4000 x 3000**	**2.77 mm**	**1.6 x 1.6 µm**
F:	1790.71		
Cx:	32.6055	B1:	0
Cy:	-31.7728	B2:	0
K1:	-0.234129	P1:	8.02272e-05
K2:	0.0606997	P2:	0.000281775
K3:	-0.00693412	P3:	0
K4:	0	P4:	0

Ground Control Points

Fig. 6. GCP locations.

Count	X error (m)	Y error (m)	Z error (m)	XY error (m)	Total (m)
3	1.62386	1.58088	0.783502	2.2663	2.39791

Table 2. Control points RMSE.
X - Easting, Y - Northing, Z - Altitude.

Label	X error (m)	Y error (m)	Z error (m)	Total (m)	Image (pix)
point 1	-0.737359	-2.14732	0.780505	2.40081	0.000 (4)
point 2	2.22663	1.60108	0.224142	2.75165	0.000 (10)
point 3	-1.55214	0.568471	-1.08729	1.97851	0.000 (6)
Total	**1.62386**	**1.58088**	**0.783502**	**2.39791**	**0.000**

Table 3. Control points.

X - Easting, Y - Northing, Z - Altitude.

Digital Elevation Model

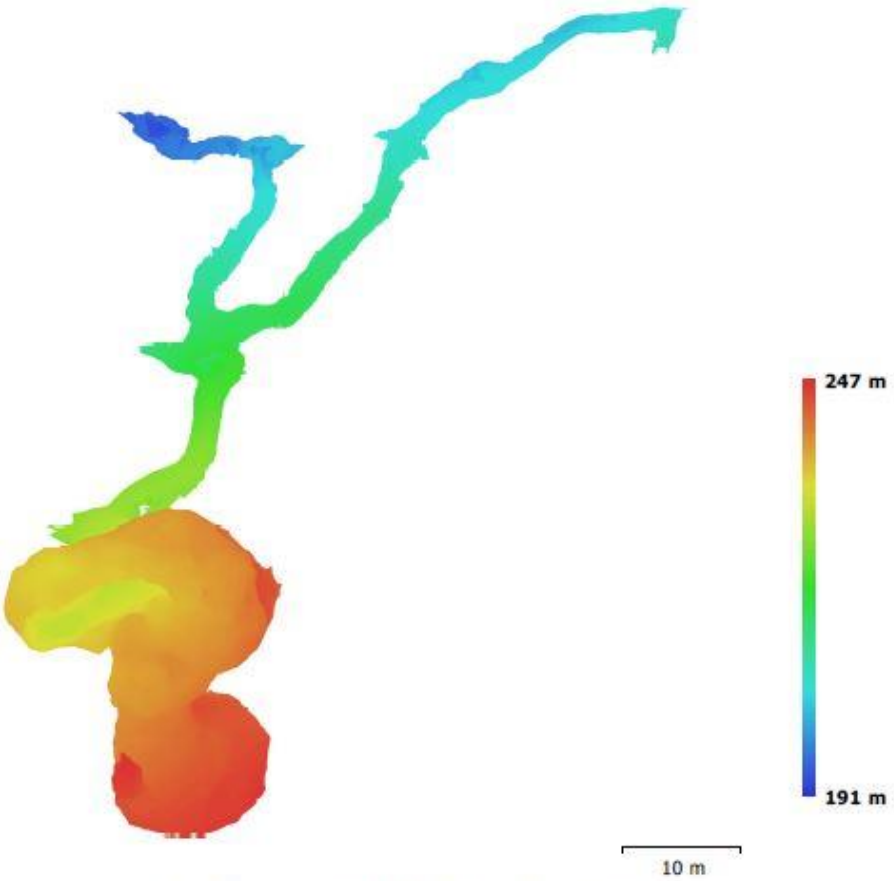

Fig. 7. Reconstructed digital elevation model.

Resolution:	4.74 mm/pix
Point density:	4.45 points/cm²

Processing Parameters

General	
Cameras	425
Aligned cameras	286
Markers	3
Coordinate system	NAD83 / Arkansas North (EPSG::26951)
Rotation angles	Yaw, Pitch, Roll
Point Cloud	
Points	219,881 of 401,486
RMS reprojection error	0.214809 (1.23308 pix)
Max reprojection error	1.06391 (46.5788 pix)
Mean key point size	5.44193 pix
Effective overlap	2.70378
Dense Point Cloud	
Points	38,476,633
Reconstruction parameters	
Quality	Medium
Model	
Faces	2,107,132
Vertices	1,063,444
Texture	4,096 x 4,096 x 4, uint8
Reconstruction parameters	
Surface type	Arbitrary
Interpolation	Enabled
Software	
Version	1.3.0 build 3772
Platform	Windows 64

Dogwood Cave

Processing Report
05 April 2017

Survey Data

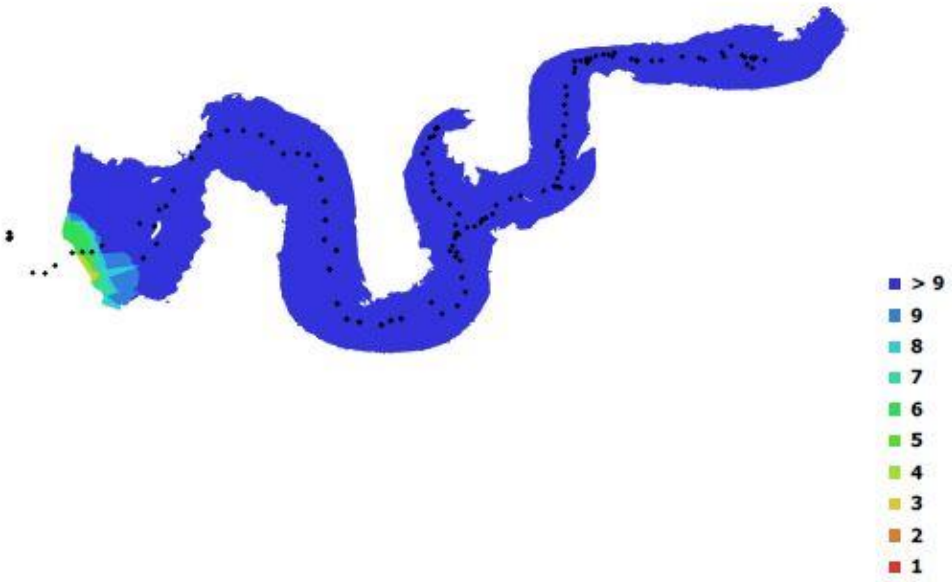

Fig. 1. Camera locations and image overlap.

Number of images:	271	Camera stations:	142
		Tie points:	97,407
		Projections:	243,561
		Reprojection error:	1.28 pix

Camera Model	Resolution	Focal Length	Pixel Size	Precalibrated
HERO3+ Black Edition (2.77 mm)	4000 x 3000	2.77 mm	1.6 x 1.6 µm	No
HERO3+ Black Edition (2.77 mm)	4000 x 3000	2.77 mm	1.6 x 1.6 µm	No
HERO3+ Black Edition (2.77 mm)	4000 x 3000	2.77 mm	1.6 x 1.6 µm	No

Table 1. Cameras.

Camera Calibration

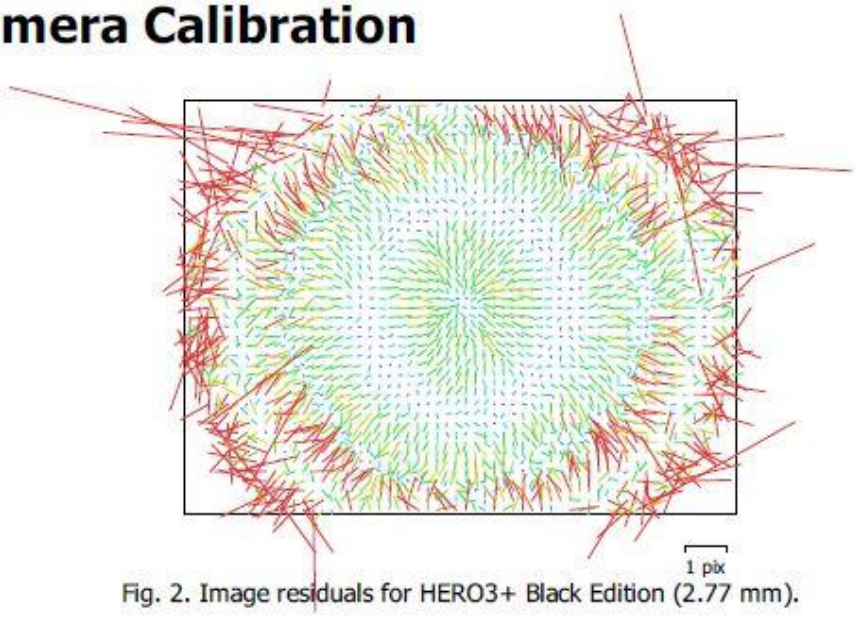

Fig. 2. Image residuals for HERO3+ Black Edition (2.77 mm).

HERO3+ Black Edition (2.77 mm)

218 images

Type	Resolution	Focal Length	Pixel Size
Frame	**4000 x 3000**	**2.77 mm**	**1.6 x 1.6 µm**
F:	1764.59		
Cx:	27.7567	B1:	0
Cy:	-3.45573	B2:	0
K1:	-0.242152	P1:	-0.00014204
K2:	0.0676884	P2:	-0.00012187
K3:	-0.00858242	P3:	0
K4:	0	P4:	0

Camera Calibration

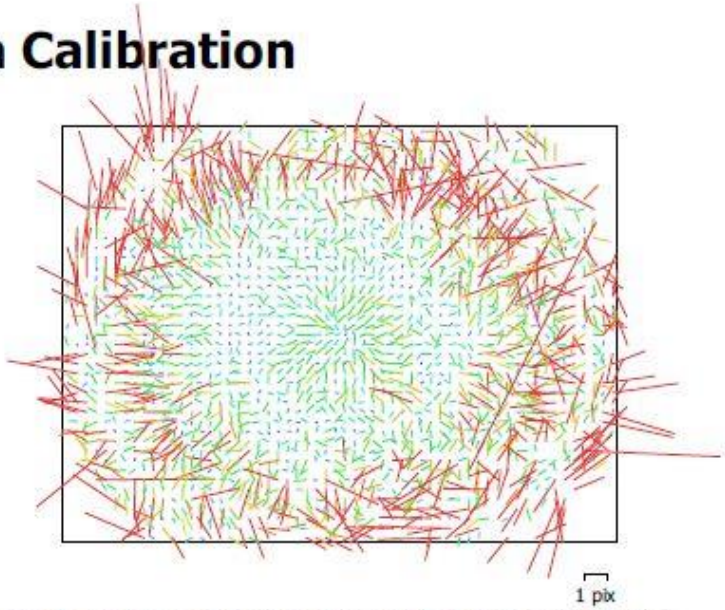

Fig. 3. Image residuals for HERO3+ Black Edition (2.77 mm).

HERO3+ Black Edition (2.77 mm)

41 images

Type	Resolution	Focal Length	Pixel Size
Frame	**4000 x 3000**	**2.77 mm**	**1.6 x 1.6 µm**

F:	1767.62		
Cx:	15.617	B1:	0
Cy:	-2.98262	B2:	0
K1:	-0.236048	P1:	-0.000100581
K2:	0.0620492	P2:	-0.000282515
K3:	-0.0073468	P3:	0
K4:	0	P4:	0

Camera Calibration

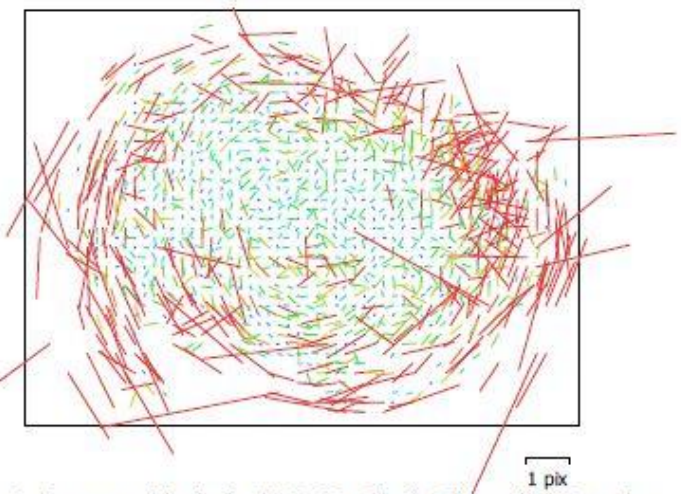

Fig. 4. Image residuals for HERO3+ Black Edition (2.77 mm).

HERO3+ Black Edition (2.77 mm)

12 images

Type	Resolution	Focal Length	Pixel Size
Frame	**4000 x 3000**	**2.77 mm**	**1.6 x 1.6 µm**

F:	1767.58		
Cx:	43.3059	B1:	0
Cy:	-9.67114	B2:	0
K1:	-0.249278	P1:	-3.31698e-05
K2:	0.0743228	P2:	3.20924e-05
K3:	-0.0094449	P3:	0
K4:	0	P4:	0

Digital Elevation Model

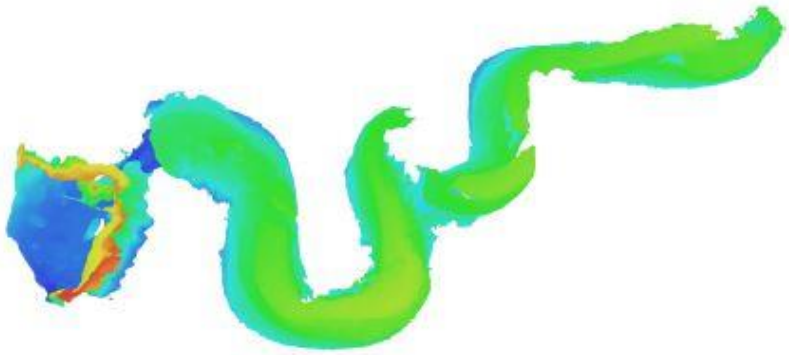

Fig. 5. Reconstructed digital elevation model.

Processing Parameters

General	
Cameras	271
Aligned cameras	142
Coordinate system	Local Coordinates (m)
Rotation angles	Yaw, Pitch, Roll
Point Cloud	
Points	97,407 of 206,848
RMS reprojection error	0.193985 (1.28131 pix)
Max reprojection error	2.88834 (39.5407 pix)
Mean key point size	6.53572 pix
Effective overlap	2.61268
Dense Point Cloud	
Points	19,211,789
Reconstruction parameters	
Quality	Medium
Model	
Faces	1,267,462
Vertices	642,883
Texture	4,096 x 4,096, uint8
Reconstruction parameters	
Surface type	Arbitrary
Source data	Dense
Interpolation	Enabled
Quality	Medium
Texturing parameters	
Mapping mode	Generic
Blending mode	Mosaic
Texture size	4,096 x 4,096
UV mapping time	1 minutes 45 seconds
Blending time	2 minutes 23 seconds
Orthomosaic	
Size	14,215 x 39,723
Coordinate system	Local Coordinates (m)
Channels	3, uint8
Reconstruction parameters	
Blending mode	Mosaic
Surface	Mesh
Enable color correction	No
Enable hole filling	Yes
Software	
Version	1.3.0 build 3772
Platform	Windows 64

UARK Utility Tunnel (Still Images)

Processing Report
11 April 2017

Survey Data

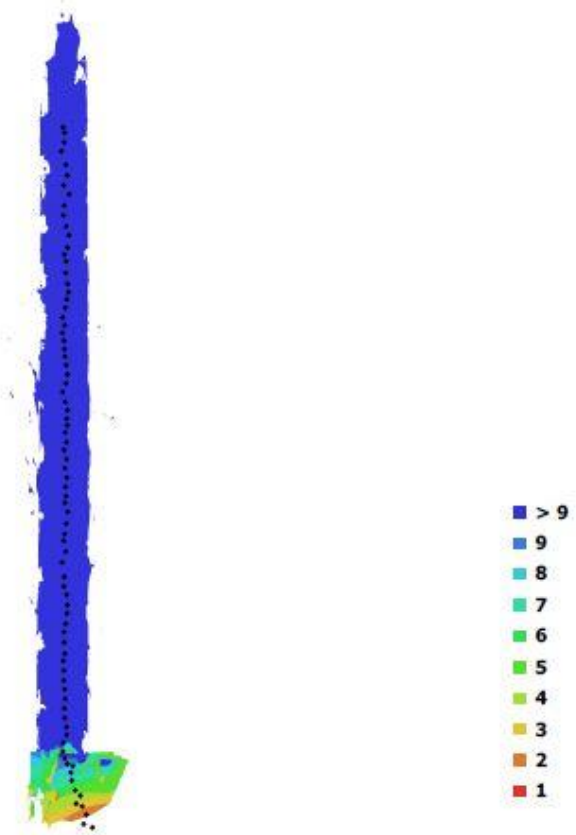

Fig. 1. Camera locations and image overlap.

Number of images:	81	Camera stations:	81
		Tie points:	42,542
		Projections:	103,289
		Reprojection error:	1.49 pix

Camera Model	Resolution	Focal Length	Pixel Size	Precalibrated
HERO3+ Black Edition (2.77 mm)	4000 x 3000	2.77 mm	1.6 x 1.6 µm	No

Table 1. Cameras.

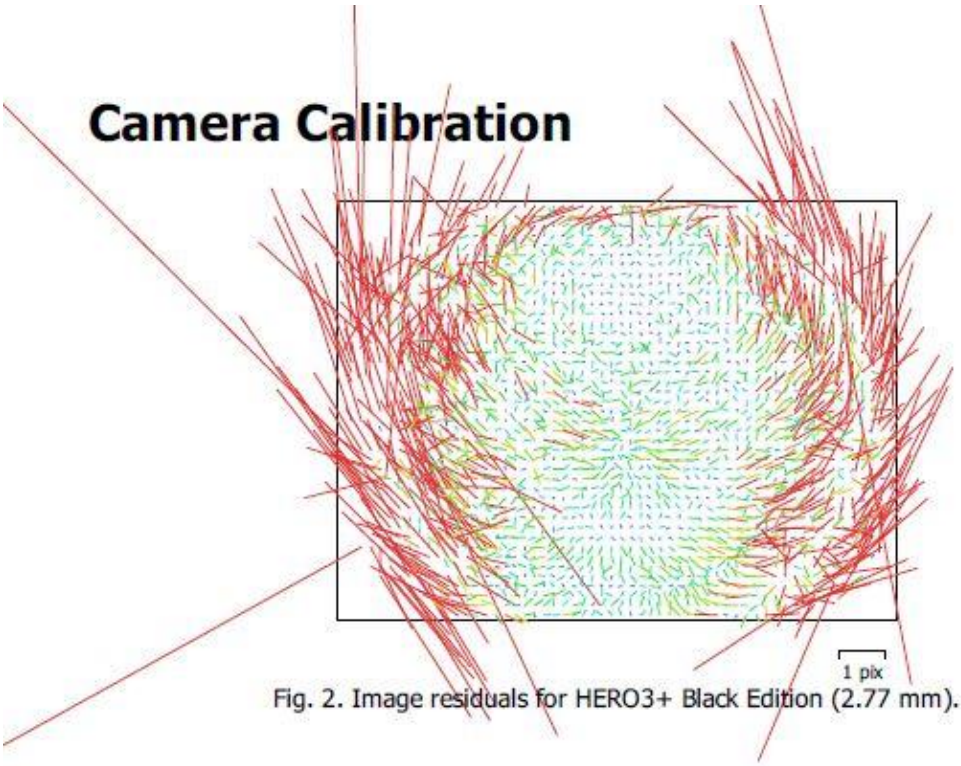

Fig. 2. Image residuals for HERO3+ Black Edition (2.77 mm).

HERO3+ Black Edition (2.77 mm)
81 images

Type	Resolution	Focal Length	Pixel Size
Frame	**4000 x 3000**	**2.77 mm**	**1.6 x 1.6 µm**

F:	1765.37		
Cx:	44.1594	B1:	0
Cy:	-12.6595	B2:	0
K1:	-0.232977	P1:	-0.000436307
K2:	0.060381	P2:	0.000215803
K3:	-0.00667353	P3:	0
K4:	0	P4:	0

Digital Elevation Model

Fig. 3. Reconstructed digital elevation model.

Processing Parameters

General	
Cameras	81
Aligned cameras	81
Markers	7
Coordinate system	Local Coordinates (m)
Rotation angles	Yaw, Pitch, Roll
Point Cloud	
Points	42,542 of 82,779
RMS reprojection error	0.201723 (1.48825 pix)
Max reprojection error	6.4268 (55.3215 pix)
Mean key point size	6.66753 pix
Effective overlap	2.73949
Alignment parameters	
Accuracy	High
Generic preselection	No
Reference preselection	No
Key point limit	40,000
Tie point limit	4,000
Constrain features by mask	No
Matching time	59 minutes 23 seconds
Alignment time	1 minutes 39 seconds
Dense Point Cloud	
Points	9,479,861
Reconstruction parameters	
Quality	Medium
Depth filtering	Moderate
Dense cloud generation time	11 minutes 28 seconds
Model	
Faces	631,989
Vertices	321,454
Texture	4,096 x 4,096, uint8
Reconstruction parameters	
Surface type	Arbitrary
Source data	Dense
Interpolation	Enabled
Quality	Medium
Depth filtering	Moderate
Face count	631,990
Processing time	19 minutes 24 seconds
Texturing parameters	
Mapping mode	Generic
Blending mode	Mosaic
Texture size	4,096 x 4,096
Enable color correction	No
Enable hole filling	Yes
UV mapping time	1 minutes 39 seconds
Blending time	1 minutes 26 seconds
Software	
Version	1.3.0 build 3772
Platform	Windows 64

UARK Utility Tunnel (Video Frames)

Processing Report
11 April 2017

Survey Data

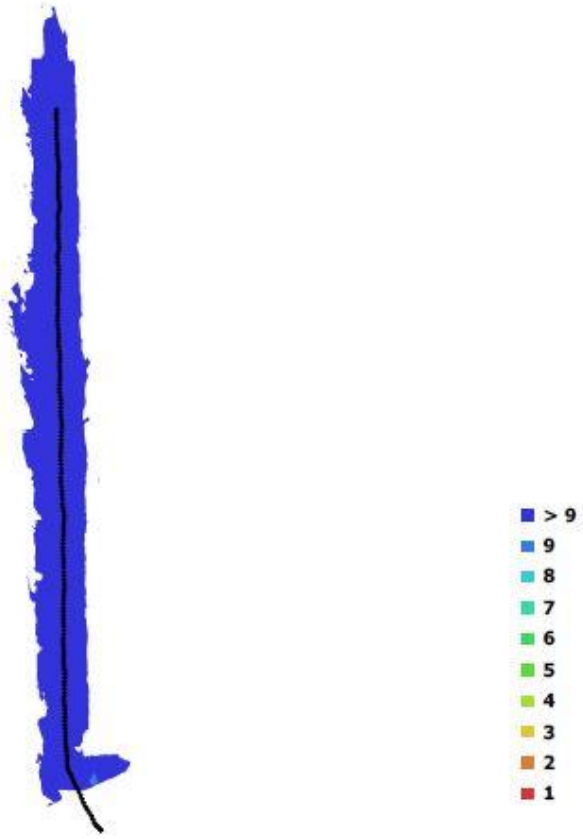

Fig. 1. Camera locations and image overlap.

Number of images:	200	Camera stations:	200
		Tie points:	58,758
		Projections:	171,602
		Reprojection error:	1.23 pix

Camera Model	Resolution	Focal Length	Pixel Size	Precalibrated
unknown	1920 x 1440	unknown	unknown	No

Table 1. Cameras.

Camera Calibration

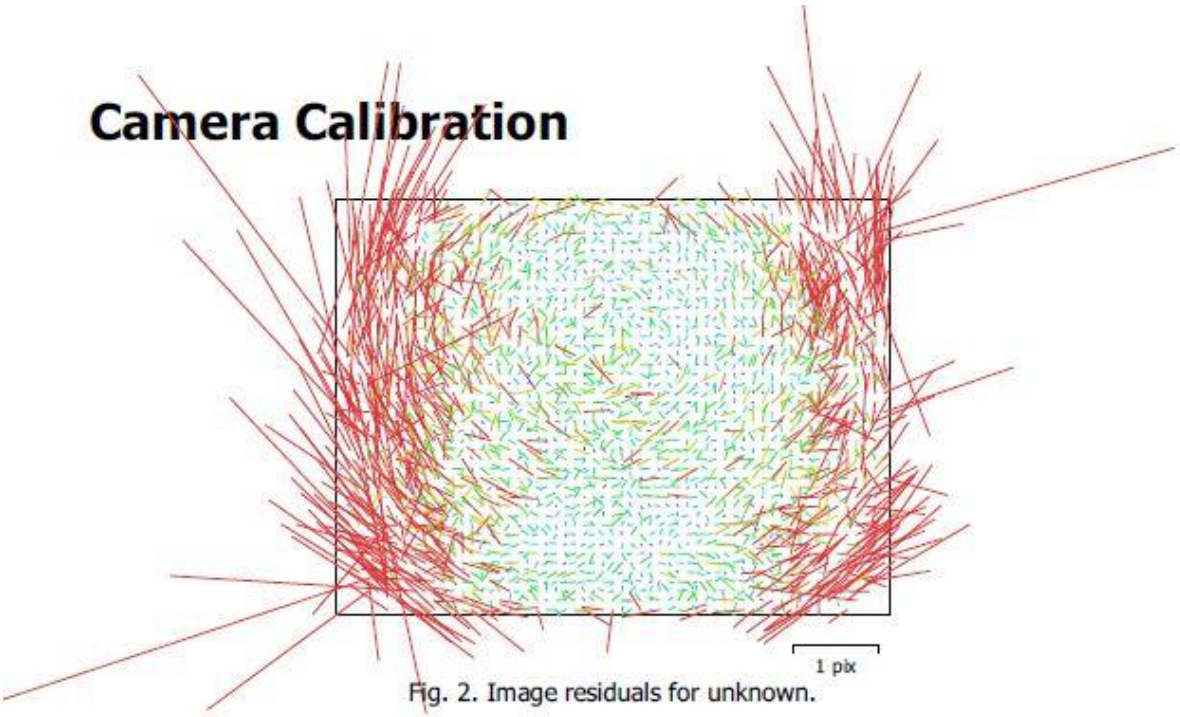

Fig. 2. Image residuals for unknown.

unknown
200 images

Type	Resolution	Focal Length	Pixel Size
Frame	**1920 x 1440**	**unknown**	**unknown**
F:	882.409		
Cx:	25.1895	B1:	0
Cy:	-3.2167	B2:	0
K1:	-0.222073	P1:	-0.00110849
K2:	0.0530836	P2:	-0.000294621
K3:	-0.00552595	P3:	0
K4:	0	P4:	0

Digital Elevation Model

Fig. 3. Reconstructed digital elevation model.

Processing Parameters

General	
Cameras	200
Aligned cameras	200
Markers	8
Coordinate system	Local Coordinates (m)
Rotation angles	Yaw, Pitch, Roll
Point Cloud	
Points	58,758 of 123,519
RMS reprojection error	0.259079 (1.23487 pix)
Max reprojection error	1.35059 (25.1942 pix)
Mean key point size	4.53309 pix
Effective overlap	3.21007
Alignment parameters	
Accuracy	High
Generic preselection	No
Reference preselection	No
Key point limit	40,000
Tie point limit	4,000
Constrain features by mask	No
Matching time	46 minutes 11 seconds
Alignment time	2 minutes 58 seconds
Dense Point Cloud	
Points	4,083,041
Reconstruction parameters	
Quality	Medium
Depth filtering	Mild
Dense cloud generation time	10 minutes 35 seconds
Model	
Faces	257,741
Vertices	130,416
Texture	4,096 x 4,096, uint8
Reconstruction parameters	
Surface type	Arbitrary
Source data	Dense
Interpolation	Enabled
Quality	Medium
Depth filtering	Mild
Face count	272,202
Processing time	6 minutes 12 seconds
Texturing parameters	
Mapping mode	Generic
Blending mode	Mosaic
Texture size	4,096 x 4,096
UV mapping time	1 minutes 17 seconds
Blending time	1 minutes 24 seconds
Software	
Version	1.3.0 build 3772
Platform	Windows 64